AMERICAN SOCIETY FOR MICROBIOLOGY | Infection and Immunity®

FUNGAL AND PARASITIC INFECTIONS

Morphological and Motility Features of the Stable Bleb-Driven Monopodial Form of *Entamoeba* and Its Importance in Encystation

Deepak Krishnan,[a] Sudip Kumar Ghosh[a]

[a]Department of Biotechnology, Indian Institute of Technology Kharagpur, Kharagpur, India

ABSTRACT *Entamoeba histolytica* and its reptilian counterpart and encystation model *Entamoeba invadens* formed a polarized monopodial morphology when treated with pentoxifylline. This morphology was propelled by retrograde flow of the cell surface resulting from a cyclic sol-gel conversion of cytoplasm and a stable bleb at the leading edge. Pentoxifylline treatment switched the unpolarized, adherent trophozoites to the nonadherent, stable bleb-driven form and altered the motility pattern from slow and random to fast, directionally persistent, and highly chemotactic. Interestingly, exogenously added adenosine produced multiple protrusions and random motility, an opposite phenotype to that of pentoxifylline. Thus, pentoxifylline, an adenosine antagonist, may be inducing the monopodial morphology by preventing lateral protrusions and restricting the leading edge to one site. The polarized form of *E. invadens* was aggregation competent, and time-lapse microscopy of encystation revealed its appearance during early hours, mediating the cell aggregation by directional cell migration. The addition of purine nucleotides to *in vitro* encystation culture prevented the formation of polarized morphology and inhibited the cell aggregation and, thus, the encystation, which further showed the importance of the polarized form in the *Entamoeba* life cycle. Cell polarity and motility are essential in the pathogenesis of *Entamoeba* parasites, and the stable bleb-driven polarized morphology of *Entamoeba* may also be important in invasive amoebiasis.

KEYWORDS cell aggregation, cell polarization, chemokinesis, encystation, pentoxifylline, stable bleb, chemotaxis

Cell migration is an important event in many physiological and pathological events, and it can be due to chemotaxis (directed migration in a gradient) or chemokinesis (random motility in response to a stimulus) (1). Directional cell migration occurs during many biological processes, such as targeting of pathogens and infection sites by immune cells, wound healing by epithelial cells, and movement of progenitor cells in the embryo, as well as in aggregative multicellularity in amoebas like *Dictyostelium discoideum*. Directional migration can be externally controlled, as in the case of chemotaxis, or it can be an intrinsic property of the cell morphology (2). Chemotaxis consists of three distinct processes: polarity, directional sensing, and motility (3, 4). Polarity refers to the redistribution of cytoskeletal components and generation of an asymmetric shape with distinct leading and trailing edges, making the cell more sensitive to chemoattractants. Directional sensing refers to the ability of cells to determine the direction of external cues like spatial gradients of chemoattractants and convert them into amplified intracellular signals. Motility involves the extension of the leading edge and retraction of the rear. Depending on the leading edge, motility can be of two types, lamellipodial motility driven by actin polymerization and pressure-driven blebbing (5). Keratocytes and fibroblasts use lamellipodia at the leading edge,

Citation Krishnan D, Ghosh SK. 2020. Morphological and motility features of the stable bleb-driven monopodial form of *Entamoeba* and its importance in encystation. Infect Immun 88:e00903-19. https://doi.org/10.1128/IAI.00903-19.

Editor De'Broski R. Herbert, University of Pennsylvania

Address correspondence to Sudip Kumar Ghosh, sudip@bt.iitkgp.ac.in.

Received 30 November 2019
Returned for modification 11 January 2020
Accepted 27 April 2020
Accepted manuscript posted online 11 May 2020
Published 21 July 2020

while primordial germ cells and amoeboid tumor cells use blebbing motility (6, 7). *Dictyostelium* cells were reported to alternate between lamellipodia and blebs, depending on the conditions (8).

Cell polarity and motility are important determinants of the pathogenicity of the enteric parasite *Entamoeba histolytica*, the causative agent of amoebiasis (9, 10). *E. histolytica* is a highly motile organism, and it has been shown to undergo chemotaxis toward enzymatic hydrolysate of casein, bacteria, and rat colon washings (11). Human tumor necrosis factor (TNF) is chemoattractant as well as chemokinetic for *E. histolytica* (12), and TNF-mediated chemotaxis has been reported to be important in pathogenesis (13). Chemicals secreted into the medium by *E. histolytica* have been shown to induce chemokinesis (14). *Entamoeba invadens* is used as an *in vitro* model to study *Entamoeba* encystation, as it readily forms cysts *in vitro* with features similar to *E. histolytica* cysts (15). During *in vitro* encystation, *E. invadens* forms large multicellular aggregates, and cysts are formed only in these aggregates. Aggregative multicellularity mediated by chemotaxis was observed in amoebas like *Acrasis*, *Copromyxa*, and *Dictyostelium* during cyst and spore formation (16). Thus, directional migration may also have a role in forming the encystation-specific multicellular structures in *Entamoeba* organisms.

E. histolytica has been reported to use only bleb-driven motility both *in vitro* and *in vivo* and thus is considered an important model to study blebbing (17). In the absence of external cues, *Entamoeba* cells form multiple protrusions randomly all around the cell, which result in continuous directional changes (17). Recently, a unique mode of prototypic amoeboid cell migration, termed stable bleb motility, has been identified in cancer cells and in the progenitor cells of zebrafish embryos (18, 19). Also, the presence of a similar migration mode called leader bleb-based migration has been observed in melanoma cells (20). Stable bleb-like protrusions were also reported in quinine-treated *Dictyostelium* cells (21), and so stable bleb motility is considered a fundamental motility mode of eukaryotic cells (18). The directionality and speed of cell movement are determined by the leading-edge protrusions, and thus, continuous membrane blebs at one point on the cell surface allow the cells to move in one direction. These cells show an elongated shape, a leading edge devoid of actin, increased migration speed and directional persistence, weak substrate adhesions, and an adhesion-independent migration propelled by nonspecific substrate friction (22). Here, we report that both the human pathogen *E. histolytica* and its reptilian counterpart and encystation model *E. invadens* also formed a similar "stable bleb" morphology when treated with millimolar concentrations of methylxanthines like pentoxifylline (Ptx) or caffeine. The Ptx-induced morphology of *Entamoeba* also showed all these characteristics, and new blebs were generated only from the preexisting leading edge, rather than in different directions around the cell as previously reported, indicating that this unique morphology is stable bleb driven. In this work, we tried to characterize its morphological and motility parameters, chemotactic potential, and morphological events during polarization and also studied its importance in encystation.

RESULTS

Methylxanthines induce polarized morphology in *Entamoeba*. The developmental pathways of the social amoeba *Dictyostelium* and the protozoan parasite *Entamoeba* have been shown to be controlled by cyclic AMP (cAMP) (23, 24). Caffeine, a nonselective phosphodiesterase inhibitor and adenosine receptor antagonist, has been widely used to study cAMP-mediated signaling in *Dictyostelium* (25), and so we tried to find whether it has any effect on *Entamoeba*. Trophozoites of the protozoan enteric parasites *E. histolytica* and *E. invadens* show an irregular shape during *in vitro* growth conditions. We observed that when exposed to millimolar concentrations (0.5 to 10 mM) of methylxanthines like caffeine or pentoxifylline (Ptx), cells of both *Entamoeba* species changed to a highly elongated morphology with a single leading edge and a trailing edge called the uroid (Fig. 1A; Movie S1 in the supplemental material). In the experiments described below, we used Ptx, as it is highly soluble in water. The Ptx-induced morphological changes were characterized by the shape descriptors as-

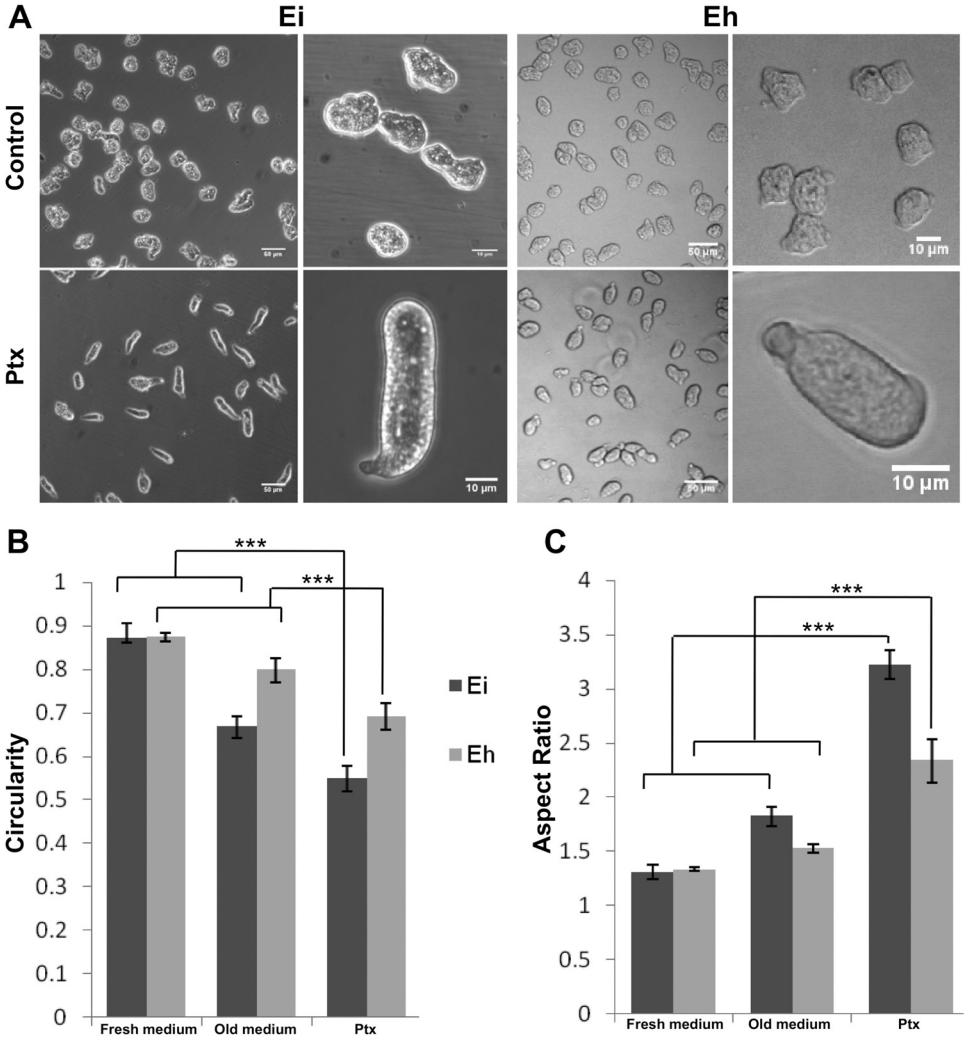

FIG 1 Pentoxifylline (Ptx) induced cell polarity in *Entamoeba*. (A) Normal (Control) and polarized (Ptx-treated) morphology of *E. invadens* (Ei) and *E. histolytica* (Eh). (B) Trophozoites in fresh growth medium showed high circularity (0.87), indicating the unpolarized nature of cells. In older medium (after 12 h of incubation) the circularity was slightly reduced, indicating the formation of protrusions. Ptx treatment significantly reduced the circularity due to front-rear polarization. (C) The morphology of the polarized cells was defined by the aspect ratio. Cells in growth medium showed an aspect ratio of 1.3, but in older medium it was higher, especially for *E. invadens* (1.8). After Ptx treatment, it changed to 2.27 in *E. histolytica* and 3.2 in *E. invadens* due to the elongated morphology. See also Movie S1 in the supplemental material. Scale bars show 50 μm or 10 μm. ***, $P < 0.001$. Data are mean values $\pm$ standard deviations (SD) for a minimum of 3 independent experiments.

pect ratio and circularity (Fig. S1). A circularity value of 1 represents a perfect circle, and unpolarized cells show high circularity (26). Cell polarization involves the breaking of symmetry due to the formation of protrusions like lamellipodia or blebs, and so low circularity was observed in migratory polarized cells. The circularity value of *E. histolytica* and *E. invadens* cells in fresh growth medium (up to 6 h after seeding) was 0.87 (Fig. 1B, Fresh medium), indicating their unpolarized state. As the growth medium became old (after 12 h of incubation), the circularity value reduced to 0.66 ± 0.02 (mean $\pm$ standard deviation) in *E. invadens* and 0.79 ± 0.02 in *E. histolytica* (Fig. 1B, Old medium), which showed the breaking of symmetry due to the formation of protrusions. Since the polarized morphology showed an elongated shape, it was characterized by the aspect ratio (ratio of the major axis to the minor axis). Both *Entamoeba* species showed an average aspect ratio of 1.3 in fresh growth medium up to 6 h after seeding (Fig. 1C, Fresh medium), but after 12 h of incubation, it increased slightly to 1.8 ± 0.09 in *E. invadens* and 1.5 ± 0.03 in *E. histolytica* (Fig. 1C, Old medium). Ptx treatment,

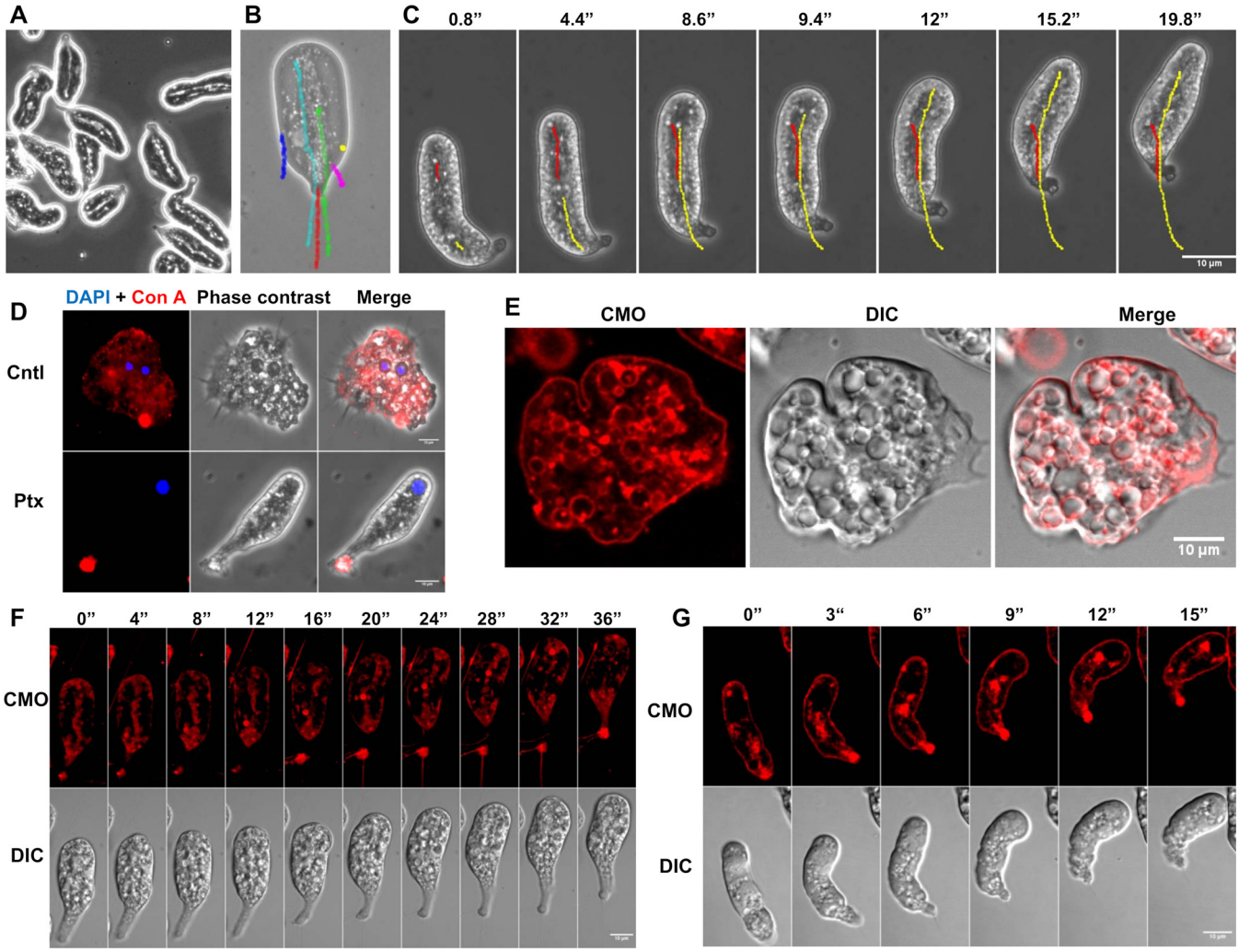

FIG 2 Rearward flow of cell surface due to sol-gel conversion propelled the polarized morphology. (A) Under a phase-contrast microscope, the cytoplasm of the polarized form of *E. invadens* was found to have granular endoplasm spanning the entire length of the cell, surrounded by a hyaline ectoplasm. (B) The trajectories of cytoplasmic particles in the endoplasm (green and cyan) and ectoplasm (blue, yellow, and pink) relative to that of the cell (red) showed that the ectoplasm was nearly stationary and the endoplasm moved fast. See also Movie S2. (C) As the particles in endoplasm reached the leading edge, they became immobilized at that point relative to the substratum, but the leading edge moved forward, which showed that endoplasmic sol became ectoplasmic gel at the leading edge. (D) Addition of Texas red-concanavalin A to unpolarized *E. invadens* cells (Cntl) stained the entire cell surface, but in polarized *E. invadens* cells (Ptx), the fluorescence accumulated at the uroid, which further indicated the rearward movement of the cell surface during migration. (E) Membrane staining with CellMask orange (CMO) showed that in unpolarized *E. invadens* trophozoites, the fluorescence was observed on the membrane and internalized vesicles. DIC, differential inference contrast. (F, G) In the polarized *E. invadens* cells, fluorescence accumulated at the uroid and in the endoplasm as a continuous posterior-to-anterior flow (F) or clumps of fluorescing vesicles moving toward the leading edge (G). See also Movie S3. Time in seconds is shown above the images. Scale bars show 10 μm.

however, significantly reduced the circularity to 0.69 ± 0.03 in *E. histolytica* and 0.54 ± 0.03 in *E. invadens* (Fig. 1B, Ptx). The aspect ratio of the Ptx-induced polarized form was 2.27 ± 0.20 in *E. histolytica* and 3.2 ± 0.13 in *E. invadens* (Fig. 1C, Ptx), indicating that front-rear polarization was more prominent in *E. invadens* than *E. histolytica*.

Sol-gel transition drives a rearward movement of the cell surface. Phase-contrast images of the polarized form indicated a clear separation of its cytoplasm into a central granular endoplasm spanning the entire length of the cell and a surrounding hyaline ectoplasm (Fig. 2A). This change in the cytoplasmic viscosity could be seen from the movement of cytoplasmic particles; the particles in the endoplasm moved very fast, while those at the cell edge were relatively stationary (Fig. 2B; Movie S2). When particles moving through endoplasm were tracked, it was observed that as soon as they reached the leading edge, they became stationary relative to the substratum, and the leading

edge moved forward (Fig. 2C). As the cell moved forward, the particles were shifted toward the trailing edge, where they again joined the endoplasmic flow. Thus, at the leading edge, the endoplasmic sol was converted into the ectoplasmic gel, which at the trailing edge was converted back into fluid endoplasm, resulting in the circulation of cytoplasm inside the cell during the cell migration. This sol-gel conversion could create a retrograde flow of the cell surface, which could be propelling the cell. When the stationary unpolarized cells were stained with fluorophore-tagged concanavalin A, the entire surface of cells was stained (Fig. 2D, Cntl [control]). However, in motile polarized morphology, the fluorescence was found to accumulate at the trailing edge (uroid) (Fig. 2D, Ptx), which indicates a retrograde flow of the cell surface. When unpolarized trophozoites were stained with the membrane stain CellMask orange (CMO), most of the fluorescence was observed on the plasma membrane and the internalized vesicles (Fig. 2E). In the polarized form, fluorescence was found mainly at the uroid and in the endoplasm (Fig. 2F and G; Movie S3). Large numbers of fluorescent vesicles were observed originating from the uroid and moving forward through the endoplasm either as a continuous flow (Fig. 2F) or as clumps (Fig. 2G), and this posterior-to-anterior flow may be replenishing the membrane at the leading edge.

The leading edge of the polarized morphology contains a stable bleb. To analyze how protrusions were formed on the control and Ptx-treated cells, the cell movements were recorded by time-lapse microscopy from which the cell outlines were extracted and overlaid. In the control cells, protrusions formed all over the cell, resulting in continuous morphological changes (Fig. 3A, Control), but in Ptx-induced polarized cells, the protrusion was restricted to the leading edge, and the overall shape of the cell did not change during the migration (Fig. 3A, Ptx). Kymographs (space-time plots) obtained from phase-contrast time-lapse movies were used to analyze the leading-edge behavior further. Unpolarized trophozoites extended and retracted protrusions even when they were moving in a straight direction, and the cell front and back moved at different rates (Fig. 3B). In cells with the polarized morphology, the protrusion at the leading edge advanced continuously and both the leading edge and the trailing edge moved at the same rate (Fig. 3C). Thus, in the Ptx-induced polarized form, protrusions were formed only at the leading edge, and to determine the nature of these protrusions, the actin cytoskeleton was stained.

Cytoplasmic microtubules are absent in *Entamoeba* organisms, and so the actin cytoskeleton alone is responsible for their morphology and motility (27). In the unpolarized *E. invadens* and *E. histolytica* trophozoites, most F-actin was found in structures like phagocytic and pinocytic invaginations and stress fibers (Fig. S2). In *E. histolytica* trophozoites, these cell surface invaginations were present at lower frequencies than in *E. invadens*, but large numbers of blebs were observed. The Ptx-induced cell polarization was characterized by drastic rearrangement of the actin cytoskeleton. F-actin was mostly localized at the uroid and the subcortical region of the cell, with its concentration decreasing from uroid to leading edge (Fig. 3D). The initial polarized form showed F-actin adhesion structures on the ventral surface (Fig. 3E), but these structures disappeared in the final form (Fig. 3F). At the leading edge of the polarized *Entamoeba* cell was a single spherical hyaline protrusion which contained the smallest amount of F-actin compared to other regions of the cell (Fig. 3E and F, arrowheads), clearly distinct from the F-actin-rich, actin polymerization-driven lamellipodial leading edge (Fig. 3G). Such an F-actin distribution and the shape of the protrusion indicated that the leading edge of the polarized form contained a bleb (8). The life cycle of a bleb involves depolymerization of the actin cytoskeleton, causing the intracellular pressure to push the membrane forward, followed by actin cortex reformation under the plasma membrane. Actin scars from such cyclic generation and healing of the actin cortex were observed at the leading edge of early polarized cells and cells performing a turn (Fig. 3H), which further confirmed the presence of a bleb at the leading edge. Thus, a continuously expanding single spherical hyaline leading edge devoid of F-actin and the occasional presence of F-actin scars indicate a bleb, and since the leading edge

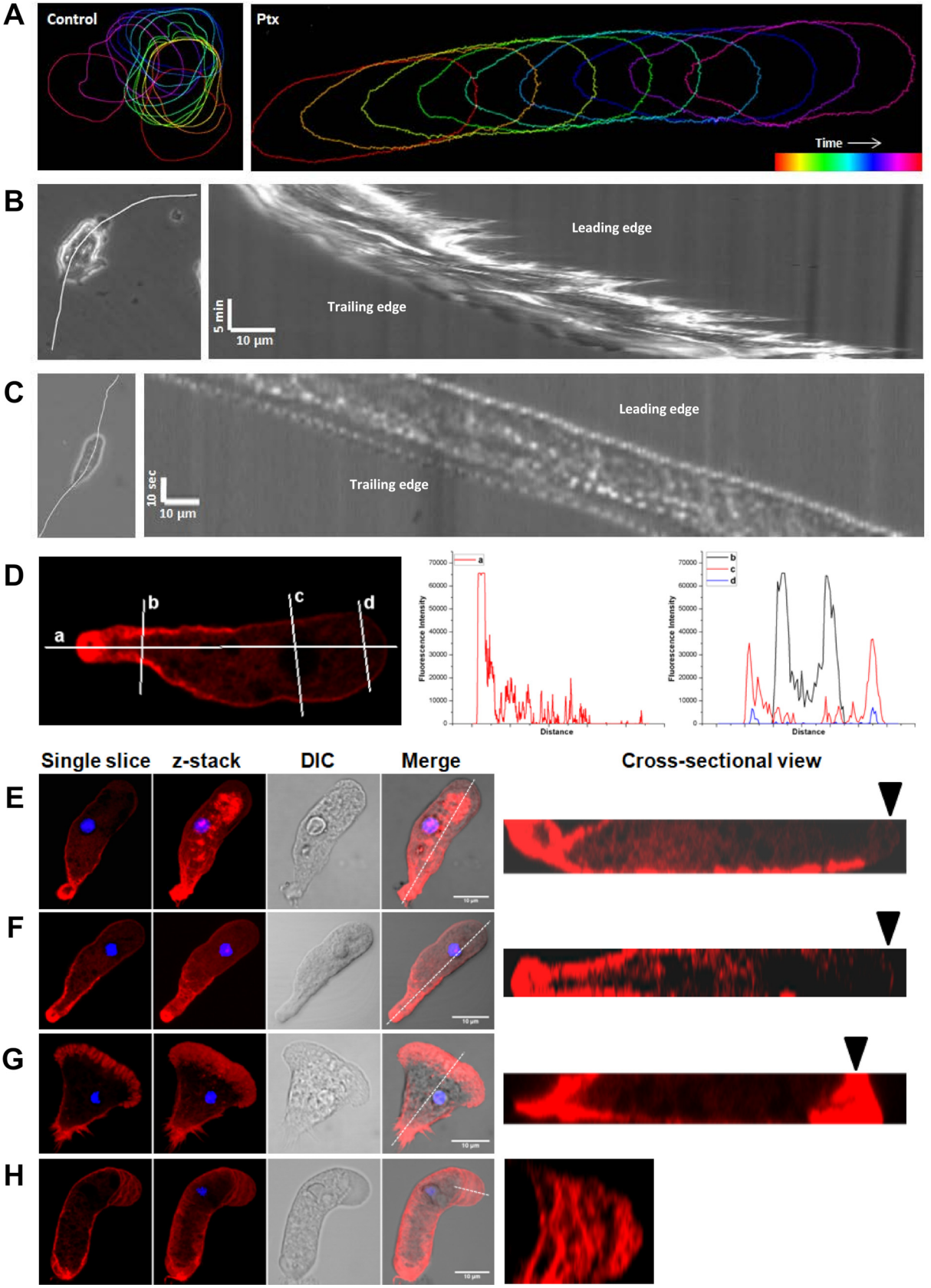

FIG 3 Leading edge of the polarized morphology contains a stable bleb. (A) Movement of unpolarized (Control) and polarized (Ptx) *E. invadens* cells shown by color-coded time sequence of cell outline. In unpolarized cells, protrusions are formed randomly all over the cell surface, but in

(Continued on next page)

contained a stabilized bleb, the migration mode is considered stable bleb driven (8, 18, 19).

The stable bleb-driven form is highly motile and directionally persistent. To compare the migrational properties of the unpolarized and polarized *Entamoeba* trophozoites, 2-dimensional (2-D) migration patterns of these forms were recorded using time-lapse video microscopy. The migrational paths of individual cells were constructed from the positions of cells at definite time points, which were then used to calculate velocity and directional persistence (28). Migration velocity was calculated as the total distance traveled by a cell divided by time. Directness, a measure of directional persistence of cell movement, is the ratio of the displacement and distance traversed by the cell during migration (Fig. S3). The directness value varies between zero and 1, with lower values indicating random migration and values near 1 indicating a cell's tendency to travel in a straight line. The velocity of unpolarized *E. histolytica* and *E. invadens* trophozoites in fresh growth medium was ~0.1 μm/s, and in 12-h-old growth medium, it increased to ~0.3 μm/s (Fig. 4A). This increase in velocity could be because of the chemokinetic effect of chemicals secreted by the trophozoites (14). Under both conditions, the cell movement was random, as observed from the low directness (*D*) values (Fig. 4B), though in *E. histolytica*, the randomness increased with velocity ($D = 0.52$ to $D = 0.33$). In the case of Ptx-induced polarized forms of *E. histolytica* and *E. invadens*, the velocity increased to nearly 1 μm/s (Fig. 4A, Ptx). Most importantly, the movement was highly directional, with a directness value of 0.7 (Fig. 4B, Ptx). These changes in the motility pattern could be seen from the 2-D migrational tracks of unpolarized and polarized *Entamoeba* cells (Fig. 4C; Movie S4).

Ptx-induced chemokinesis and enhanced chemotaxis in *Entamoeba*. Ptx altered the 2-D motility pattern when added uniformly to the cells, indicating that its action is due to chemokinesis. Chemical stimuli that can cause chemokinesis sometimes also induce chemotaxis when applied as a gradient (29, 30). A transwell migration assay was carried out to find whether *Entamoeba* underwent chemotaxis toward Ptx. To stimulate the chemotaxis, Ptx was added to the bottom chamber of the transwell plate at different concentrations to generate a gradient. In separate experiments, Ptx was also added to the top chamber to stimulate chemokinesis for comparison. The cell migration was found to increase dose dependently in both cases, but it was much higher when Ptx was added to the upper chamber (at 10 mM and above, Ptx reduced transwell migration due to extensive cell aggregation in the upper chamber, as discussed below), indicating that the Ptx effect was due to chemokinesis (Fig. 5A). When the transwell migrations of the polarized and unpolarized forms of *E. histolytica* and *E. invadens* were compared, unpolarized *E. histolytica* cells showed 4-fold more migration than unpolarized *E. invadens* cells (Fig. 5B, Control). However, there was no significant difference in the migration of their polarized stable bleb forms (Fig. 5B, Ptx). Also, the Ptx-induced differences in the migrational properties of unpolarized and polarized forms were much more significant in *E. invadens* (9-fold) than in *E. histolytica* (2-fold).

Factors that increase morphological polarity and directional persistence have been shown to promote chemotaxis (2, 31). To find the chemotactic potential of polarized stable bleb-driven cells, the migration of Ptx-treated, serum-starved *Entamoeba* tro-

FIG 3 Legend (Continued)
polarized cells, single protrusions were limited to the leading edge. (B) Kymographs were generated from cell paths depicted by white lines to analyze the leading-edge behavior of unpolarized and polarized cells. Unpolarized *E. invadens* trophozoites extended and retracted protrusions, and the cell front and back moved at different rates. (C) In the polarized form of *E. invadens*, the protrusion at the leading edge formed continuously and the leading edge and the trailing edge moved at the same rate. (D) Cellular localization of F-actin in the polarized *E. invadens* cell shown by rhodamine-phalloidin staining. Fluorescence intensity across the drawn lines (a, b, c, d) shows that in the polarized form, actin was found mainly in the uroid and subcortical regions. Actin fluorescence intensity decreased toward the leading edge, which was mostly devoid of F-actin. (E) As the polarized morphology first formed, actin-based adhesion structures were observed on the ventral side of the cell. (F) By 8 to 12 h after Ptx treatment, the polarized form was completely devoid of any adhesion structures. (G) Lamellipodial motility of *Entamoeba* characterized by actin-rich protrusions (arrowhead) is shown for comparison. (H) F-actin scars at the leading edge observed in cells undergoing turning, which shows that the actin cortex is continuously stabilized and destabilized at the leading edge. A single spherical leading edge nearly devoid of F-actin and the occasional presence of F-actin scars indicate that the motility of the polarized form of *Entamoeba* is stable bleb driven. Scale bars shows 10 μm.

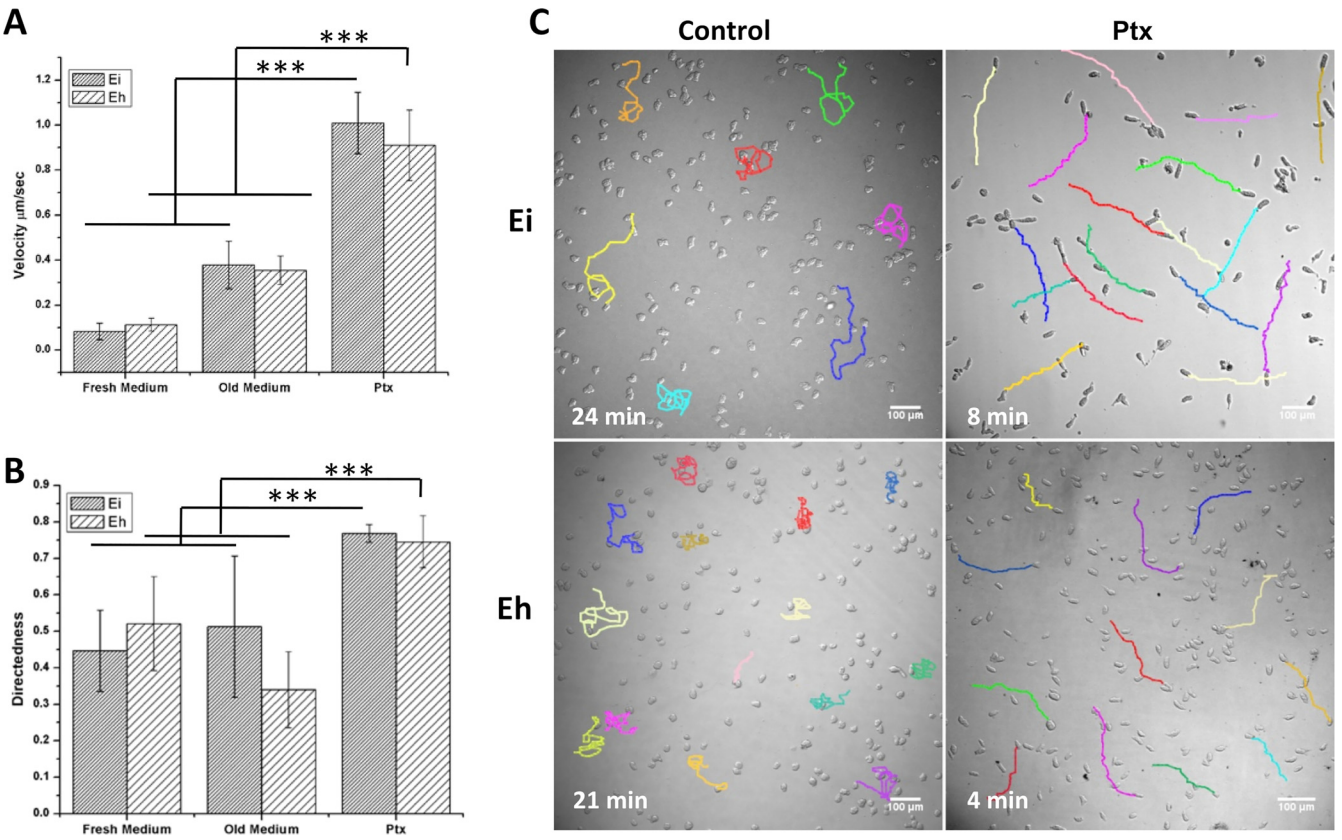

FIG 4 2-D motility characteristics of the pentoxifylline (Ptx)-induced polarized morphology. (A) *E. histolytica* and *E. invadens* trophozoites in fresh growth medium showed a velocity of ~0.1 μm/s, and in old medium, the velocity was nearly 0.4 μm/s. After Ptx treatment, the velocity increased to ~1.0 μm/s. (B) The cell movement was random in growth medium, as shown by the directness values of 0.3 to 0.5. The Ptx-induced polarized morphology showed a high directness value, indicating directional persistence. (C) The tracks of randomly chosen, individual *E. histolytica* and *E. invadens* trophozoites (colored lines) before and after Ptx treatment. See also Movie S4. Scale bars show 100 μm. Time in minutes is shown. Data are mean values ± SD for a minimum of 3 independent experiments. ***, $P < 0.001$.

phozoites toward serum-containing medium was studied using a transwell migration assay. In comparison to normal motility (serum-containing medium in both top and bottom chambers), serum-starved cells showed an increase in transwell migration, indicating chemotaxis toward serum-containing medium (Fig. 5C, 0 mM). Ptx further increased this chemotaxis dose dependently, though the Ptx effect on chemotaxis was much more significant in *E. invadens* than in *E. histolytica* (Fig. 5C, 1 and 5 mM). Thus, the Ptx action on *Entamoeba* was due to chemokinesis, but it also enhanced the chemotaxis by imparting cell polarity and stabilized bleb.

Intermediate morphological phenotypes during cell polarization. Ptx induced cell polarization at concentrations of 0.5 mM to 10 mM, and a fluorescein diacetate (FDA) hydrolysis assay showed that even at a high Ptx concentration (10 mM), cell viability was not affected up to 72 h (Fig. S4). The cell polarization in *E. invadens* trophozoites depended on the Ptx concentration, which can be seen from the changes in aspect ratio with time (Fig. 6A). At lower Ptx concentrations (0.5 to 1 mM), the cell polarization took nearly 6 to 8 h, but with higher Ptx concentrations (5 to 10 mM), the polarization was instantaneous (Fig. S5). The analysis of morphological changes in *E. invadens* cells by actin staining showed that 1 to 2 h after the addition of 1 mM Ptx, the phagocytic and pinocytic invaginations on the cell surface (Fig. 6Ba and a′) started to disappear and F-actin polymerization-based lamellipodia started appearing (Fig. 6Bb and b′). By 4 h, the lamellipodia became more and more prominent until a polarized form with a lamellipodium at the leading edge was formed (Fig. 6Bc and c′). Like the bleb-driven amoeboid form, the lamellipodium-containing form represented another polarized morphology of *Entamoeba*. By 6 h, blebs started appearing at the leading

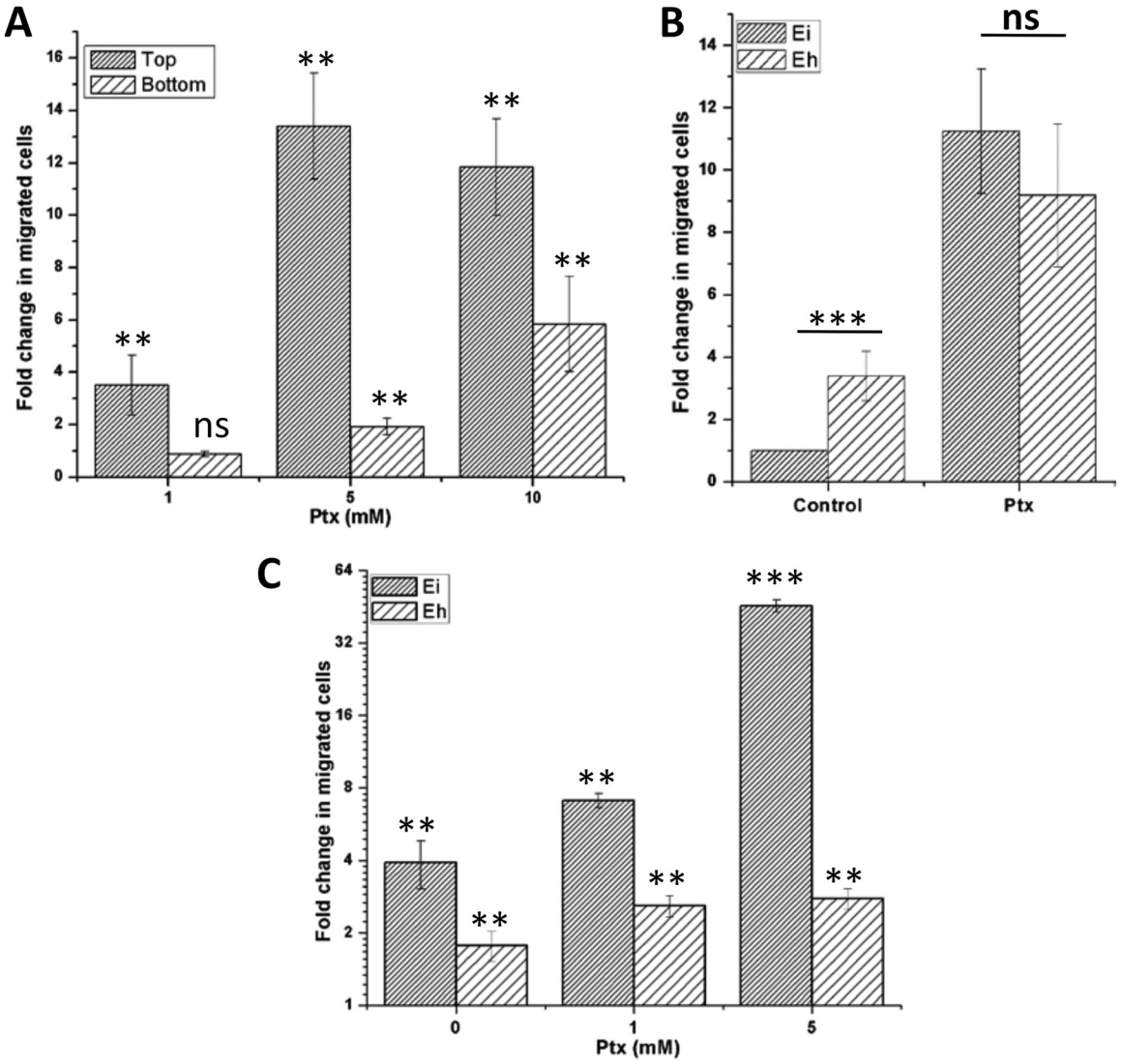

FIG 5 Effect of pentoxifylline (Ptx) on chemokinesis and chemotaxis. (A) To find whether Ptx was chemokinetic or chemotactic in *E. invadens*, it was alternatively added to the top and bottom wells of transwell chambers and the numbers of migrated *E. invadens* cells were counted. Compared to the normal migration of the untreated control, Ptx enhanced the migration much more when added to the upper chamber than to the lower chamber, indicating a chemokinetic effect. The values are shown as fold changes of the migration relative to the untreated control migration. (B) Unpolarized *E. histolytica* trophozoites were 4-fold more migrational than *E. invadens* trophozoites, but their polarized forms showed similar migration rates. The values are fold changes of the migration relative to the untreated *E. invadens* migration, which was arbitrarily set to 1. (C) Ptx also increased chemotaxis of serum-starved cells toward serum-containing medium, and the effect was much more significant in *E. invadens* than in *E. histolytica*. The values are fold changes of the chemotactic migration (serumless medium → serum-containing medium) relative to the normal migration (serum-containing medium → serum-containing medium). Data are mean values ± SD for a minimum of 3 independent experiments. *, $P < 0.05$; **, $P < 0.01$; ***, $P < 0.001$; ns not significant.

edge of the lamellipodial morphology (Fig. 6Ca, a′, b, and b′), and by 6 to 8 h, the blebs became prominent and the cells attained an elongated shape. Actin-based adhesion structures, similar to the actin feet of *Dictyostelium* (32, 33), were found on the ventral side of these initial bleb-driven cells (Fig. 6Cc, c′, d, d′, e, and e′). The adhesion structures disappeared by 8 to 12 h, giving rise to adhesion-independent, stable bleb-driven morphology (Fig. 6Cf and f′).

At a higher Ptx concentration, the morphological changes in *E. invadens* occurred faster. Time-lapse video microscopy showed that within minutes after the addition of 10 mM Ptx, *E. invadens* formed multiple protrusions all around the cell, resulting in random movement (Fig. 6D). After 2 h, a trailing edge appeared, and the multiple protrusions fused into a single leading-edge protrusion. Actin staining showed that

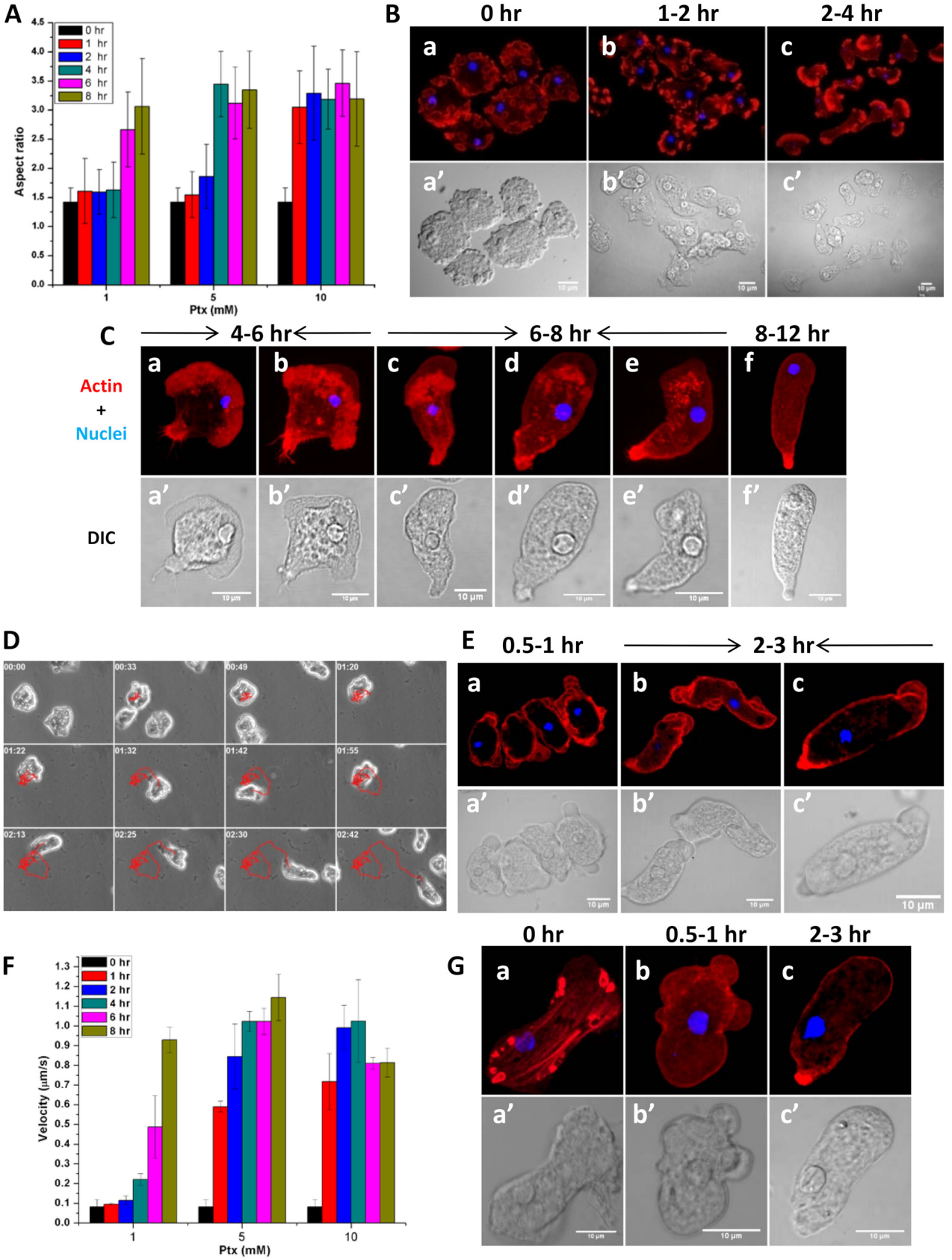

FIG 6 Morphological changes during pentoxifylline (Ptx)-induced polarization. (A) Time course of aspect ratio showed that Ptx dose-dependently induced cell polarization in *E. invadens*. (B) In the unpolarized *E. invadens* cells, the actin is found in the phagocytic and pinocytic invaginations (a, a').

(Continued on next page)

these protrusions were blebs (Fig. 6Ea and a′), which became smaller as the cell polarized (Fig. 6Eb and b′) and became confined to the leading edge by 2 to 3 h after the addition of 10 mM Ptx (Fig. 6Ec and c′). These morphological changes in response to low and high Ptx concentrations could also be observed in the increment in cell velocity with time (Fig. 6F). To achieve a similar morphological transition in *E. histolytica*, a higher Ptx concentration (5 to 10 mM) was required than for *E. invadens* (0.5 to 1 mM). In *E. histolytica* cells, the intermediate lamellipodial form was not seen, and the adherent cells (Fig. 6Ga and a′) produced multiple blebs (Fig. 6Gb and b′) in response to Ptx and directly formed the stable bleb-driven morphology (Fig. 6Gc and c′). Thus, the outcome of the Ptx-induced polarization is the conversion of unpolarized, adherent trophozoites to nonadherent, polarized, and stable bleb-driven cells. The loss of adhesion structures caused the stable bleb-driven cells to slip during later hours, which could be seen in live-cell video microscopy and also by the reduction in velocity at higher Ptx concentration (Fig. 6F, 10 mM).

The stable bleb-driven form is highly motile under confinement. Ptx dose-dependently reduced the cell adhesion (Fig. 7A), since the F-actin-based adhesion structures disappeared during the cell polarization. It has been shown previously that the adhesion-deficient cells showed normal locomotion and chemotaxis under confinement (34). The under-agarose assay has been used to study *Entamoeba*'s motility, as it provides the restrictive conditions faced by the parasite during invasive disease (14). For this, Ptx was mixed with agarose to form a uniform concentration, and the trophozoites were then added to a single trough cut in the agarose (Fig. S6). Both *E. histolytica* and *E. invadens* trophozoites spontaneously exited from the troughs and moved under the agarose. Under the agarose, the velocity of both *E. histolytica* and *E. invadens* cells was found to be $\sim$1 μm/s, even in the absence of Ptx (Fig. 7B, control). The multinucleated giant cells of *E. invadens* have shown a similar abrupt increase in cell velocity under confinement (35), and this could be due to the induction of faster bleb-driven movement by mechanical resistance (8). While velocity increased, motility remained random, with directness values of 0.60 and 0.49 for *E. invadens* and *E. histolytica*, respectively (Fig. 7C, control). However, when Ptx was present in the agarose, the velocity was further increased to 1.9 μm/s in *E. invadens* cells and to 1.69 μm/s in *E. histolytica* cells (Fig. 7B, Ptx), and the motility became highly directional ($D = 0.8$) in both *E. histolytica* and *E. invadens* cells (Fig. 7C, Ptx). Also, under agarose, the polarized *E. invadens* cells were always found to move collectively after the cells aligned with neighbors in head-to-tail fashion (Fig. 7D; Movie S5), similar to streaming in *Dictyostelium* organisms (36). The polarized *E. invadens* cells did not show such movement in a culture medium. Also, the collective movement was not observed in *E. histolytica* cells, either under confinement or in the medium.

Pentoxifylline acts as an adenosine antagonist and prevents lateral protrusions to produce the monopodial morphology. The biological effects of Ptx are either mediated by its action on adenosine receptors or due to inhibition of phosphodiesterases. Since the addition of cell-permeable dibutyryl-cyclic AMP (cAMP) did not induce cell polarization, the effects of Ptx may be mediated by adenosine receptors that are not yet identified; therefore, we studied the effect of adenosine on cell morphology and motility. Like Ptx, adenosine (0.1 to 1 mM) was also found to be

FIG 6 Legend (Continued)
After 1 h of 1 mM Ptx treatment, these phagocytic invaginations started disappearing and lamellipodia started appearing (b, b′). Lamellipodia became very prominent by 4 h, and phagocytic invaginations completely disappeared (c, c′). (C) By 4 to 6 h, blebs appeared on the lamellipodial form (a, a′, b, b′) and became prominent as the cell became elongated in shape by 6 to 8 h (c, c′, d, d′, e, e′). These polarized cells had large numbers of actin adhesion structures on their ventral surface which disappeared by 8 to 12 h, giving rise to the adhesion-independent, stable bleb-driven morphology (f, f′). (D) Time-lapse images showing the response of *E. invadens* to 10 mM Ptx. The motility track showed that the cell moved randomly at first and then became directional. (E) In response to the higher Ptx concentration (10 mM), large numbers of blebs appeared instantaneously all over the cell (a, a′), which then assumed the elongated morphology without going through the lamellipodial form (b, b′). The blebbing was finally confined to the leading edge alone (c, c′). (F) These morphological changes were observed in the increased velocity with time after Ptx treatment. (G) *E. histolytica* required the high Ptx concentration (10 mM) for polarization, and the adherent *E. histolytica* trophozoites (a, a′) formed multiple blebs on the surface (b, b′) and then formed the stable bleb morphology (c, c′). Scale bars show 10 μm. Data are mean values $\pm$ SD for a minimum of 3 independent experiments.

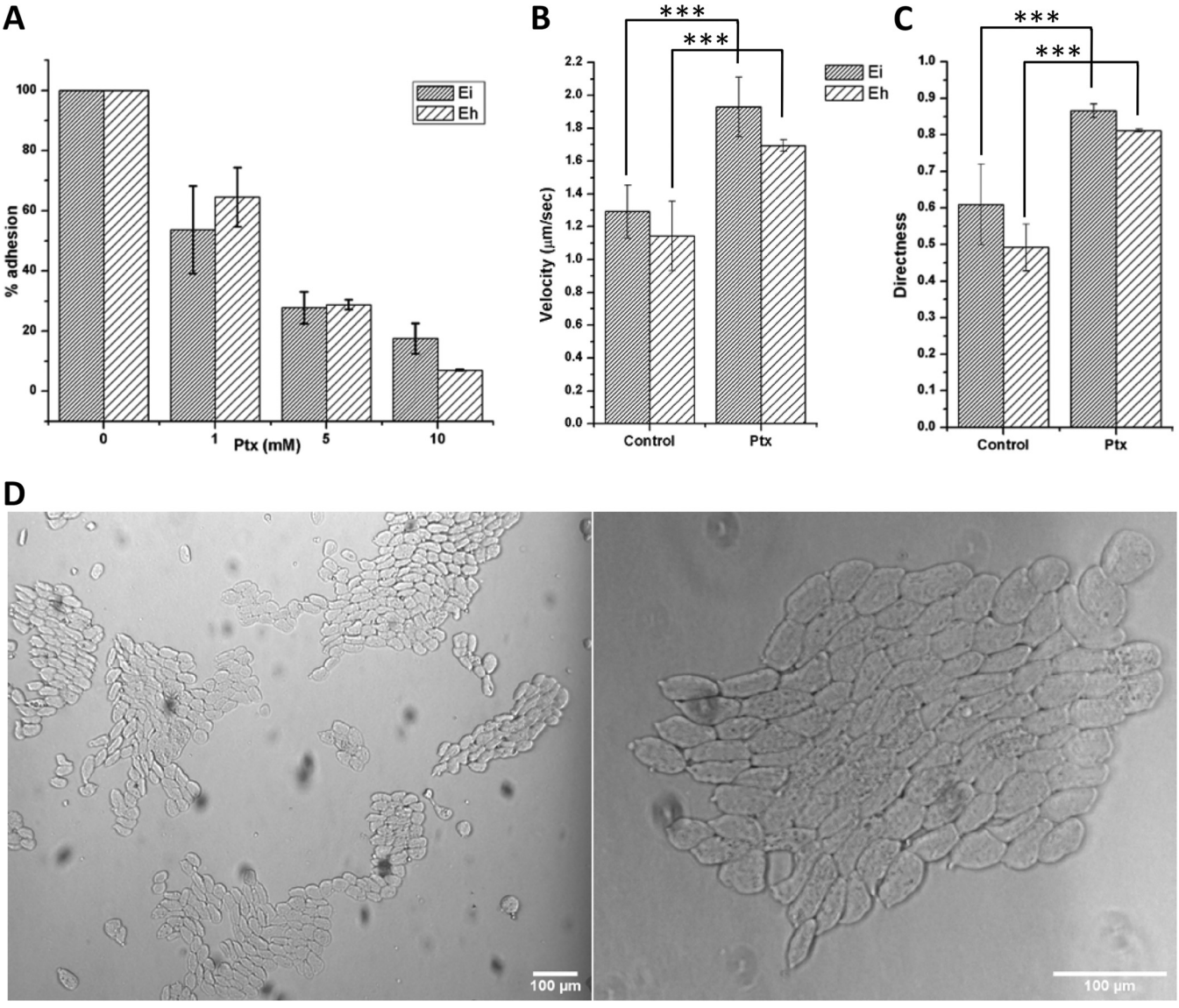

FIG 7 The adhesion-deficient stable bleb-driven form is highly motile under confinement. (A) Ptx dose-dependently reduced cell adhesion as actin-based adhesion structures disappeared during cell polarization. The number of adherent cells in the untreated control was arbitrarily set to 100%, and the values from Ptx treatment are reported as percentages of this value. (B) *Entamoeba* trophozoites became highly motile under agarose, with velocity increasing above 1.0 μm/s, but in the presence of Ptx, the velocity nearly doubled. (C) While velocity increased under agarose, motility was not directional, as observed from the directness value of 0.5 to 0.6, and with Ptx, the motility became highly directional. (D) In the presence of Ptx, the polarized *E. invadens* cells moved collectively in a head-to-tail alignment under agarose. See also Movie S5. Scale bars show 100 μm. ***, $P < 0.001$. Data are mean values $\pm$ SD for a minimum of 3 independent experiments.

chemokinetic in *E. invadens*, as it increased cell velocity to 0.50 μm/s (Fig. 8A). The most crucial feature of adenosine-induced chemokinesis was the highly random movement, which can be seen from the low directness value of 0.3 (Fig. 8B) and the migration tracks (Fig. 8C; Movie S6). The cause of such random movement was found to be the formation of protrusions all over the cell surface (Fig. 8D and E), which can also be observed from the reduction in the circularity value (Fig. 8F) after adenosine treatment. These protrusions formed all over the cell continuously (Fig. 8G), resulting in reduced net motility. Rhodamine-phalloidin staining showed that these protrusions were membrane blebs (Fig. 8H). These observations made in *E. invadens* were not visible in *E. histolytica* due to its isotropic blebbing and inherent random motility (Fig. 8A and B).

The addition of adenosine to polarized *E. invadens* cells reversed their morphological and motility features (Fig. 9A and B). In the presence of adenosine, the stable bleb-

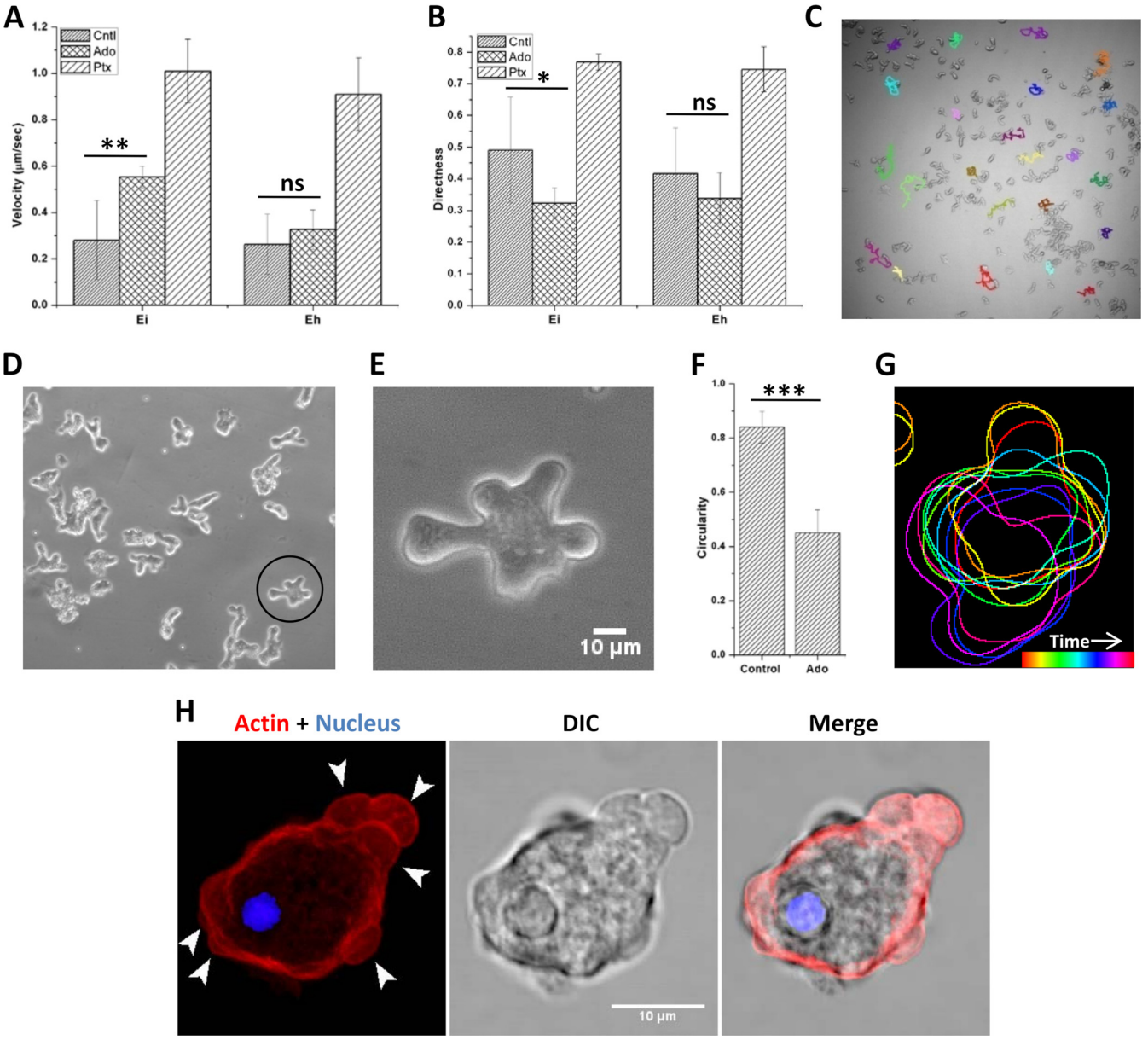

FIG 8 Adenosine induces motility characteristics opposite to those induced by pentoxifylline. (A, B) Comparison of velocities (A) and directness values (B) of unpolarized control, adenosine (Ado)-treated, and Ptx-treated *E. invadens* and *E. histolytica* cells. (C) Migratory tracks of adenosine-treated *E. invadens* cells showing the highly random movement. (D, E) Multiple protrusions formed all over the adenosine-treated *E. invadens* cells. (F) The formation of protrusions was also observed from the reduction in circularity value. See also Movie S6. (G) Color-coded time sequence of cell outline showing formation of multiple protrusions resulting in random movement. (H) Actin staining showed these protrusions were blebs (arrowheads). Scale bar shows 10 μm. *, $P < 0.05$; **, $P < 0.01$; ***, $P < 0.001$; ns not significant.

driven cells lost their polarity and produced multiple blebs, causing their directionally persistent movement to become random (Fig. 9B). These changes were also reflected in the circularity and aspect ratio (Fig. 9C). With the addition of adenosine, the aspect ratio started decreasing, and circularity started increasing as the cells gradually lost polarity. Later, due to the formation of multiple protrusions, the circularity decreased and the aspect ratio increased slightly. These observations show that the effects of adenosine treatment were precisely opposite to those of Ptx, indicating that both could be binding to the same target, which is yet to be identified. Simultaneous stimulation of these unidentified targets for adenosine produced multiple leading edges, causing the cell to move in opposing directions (Fig. 9D), and so there was no productive cell motility. In contrast, Ptx treatment produced a single leading edge, resulting in a

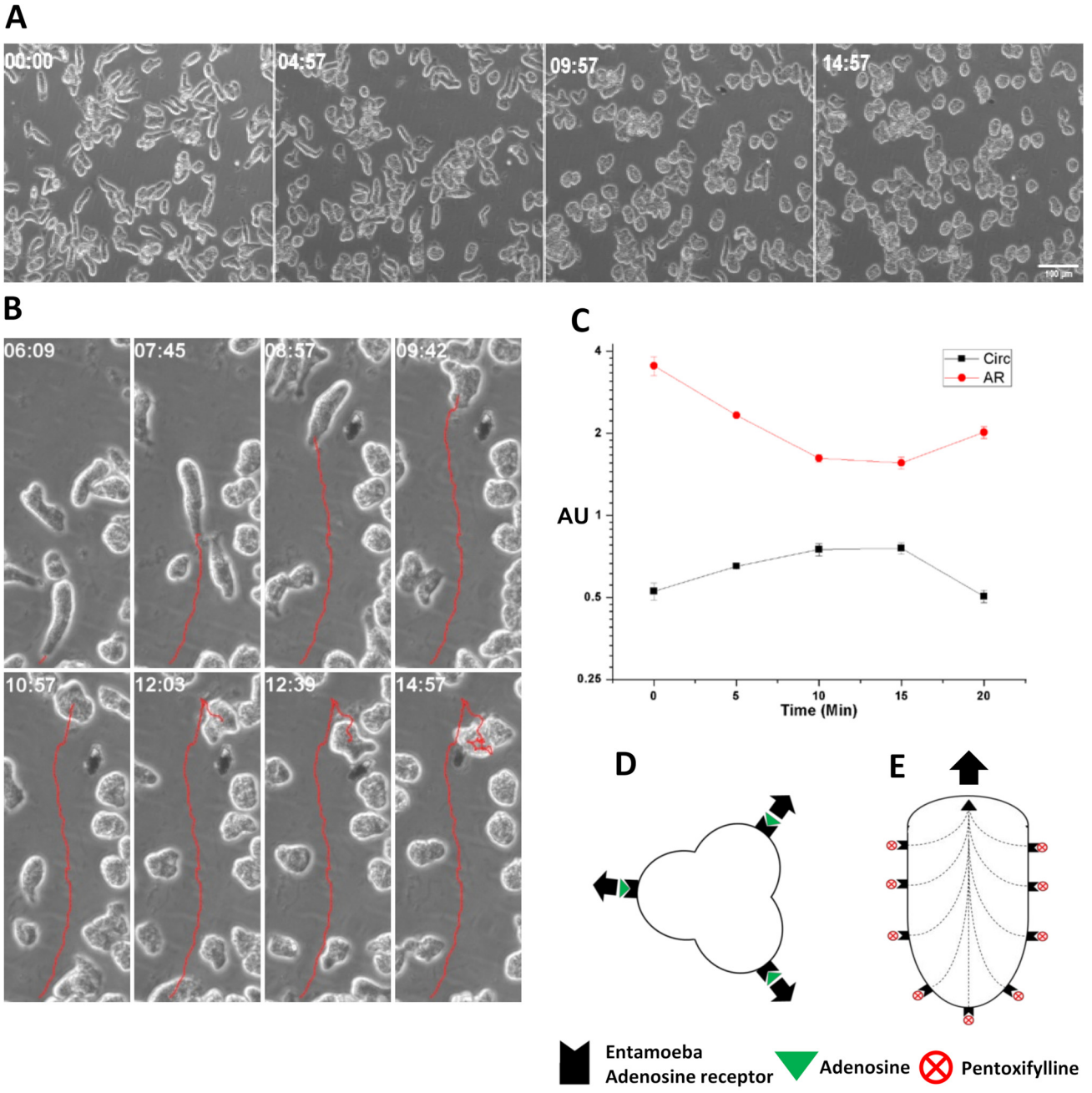

FIG 9 *E. invadens* motility pattern in response to adenosine and pentoxifylline. (A) The addition of adenosine to polarized cells reversed the morphological polarity. (B) In the presence of adenosine, the directionally persistent stable bleb-driven form lost its polarity, produced multiple protrusions, and started

(Continued on next page)

polarized morphology and causing the cell to move in a single direction (Fig. 9E). In *Entamoeba*, motility patterns in response to Ptx and adenosine represented two extremes of *Entamoeba* morphology, and the motility of trophozoites in growth medium over a long time showed elements of both randomness and directional persistence (Fig. 9F).

Role of stable bleb-driven morphology in encystation. In the model organism *E. invadens*, axenic *in vitro* encystation can be induced by a combination of nutrient and osmotic stress (37). Generally, the *in vitro* encystation protocol involves detaching the cells by chilling and washing the cells and then resuspending them in encystation medium at a cell density of 10^5 cells/ml, and it yields 80% to 90% encystation efficiency after 72 h of incubation. One of the first noticeable events in the *in vitro* encystation is the formation of galactose ligand-mediated multicellular aggregates during the early hours, and only in these aggregates do cysts form (38). Interestingly, Ptx-induced polarized cells of *E. invadens* were also able to form cell aggregates in a dose-dependent manner even in the growth medium (Fig. 10A and B). In the presence of a high Ptx concentration (10 mM), polarized *E. invadens* cells were able to form cell aggregates at a low cell density (10^3 cells/ml), indicating the aggregation competency of the stable bleb-driven polarized cells (Fig. 10C). Like the encystation-specific cell aggregates, these structures were also galactose ligand mediated, as the addition of 10 mM galactose caused instant disaggregation (Fig. 10D). While the encystation medium was capable of inducing cell aggregation in *E. invadens*, the addition of Ptx to the encystation culture was found to enhance cell aggregation further (Fig. 10E and F).

During *E. invadens* encystation, cysts appeared only inside cell aggregates, and when Ptx-induced cell aggregates in encystation medium were probed with the chitin-binding dye calcofluor white (CFW), cysts were visible in such structures (Fig. 10G). These cysts showed a complete chitin wall, four nuclei, and a chromatoid body, indicating that they have all three major characteristics of mature cysts (Fig. S7). The time course of encystation after treatment with different Ptx concentrations showed that the cyst yield increased up to 1 mM Ptx, but higher concentrations reduced encystation efficiency (Fig. 10H). The stimulatory effect of Ptx was more prominent during the early hours and could be the result of the enhanced cell aggregation. The source of galactose ligands mediating cell aggregation is unclear and is thought to be provided by the adult bovine serum in the encystation medium (39) or by the galactose-containing cyst wall protein Jacob (40). In the absence of serum, the encystation was inefficient ($<$5%), but the addition of Ptx to serumless encystation medium significantly increased the cyst formation, with encystation efficiency being highest at 1 mM ($>$50%) (Fig. 10I). Thus, apart from inducing cell polarity, Ptx also made the *E. invadens* cells aggregation competent, and therefore, the possibility of stable bleb-driven cells mediating cell aggregation during *in vitro* encystation was investigated.

To find whether the encystation stimuli also caused cell polarization, *E. invadens* cells were grown in cell culture plates, the growth medium was replaced with encystation medium, and the response of the cells was recorded with time-lapse video microscopy. Similar to the results of the Ptx stimulation, the cells became polarized and highly motile (Fig. 11A; Movie S7). Confluent cultures usually contained spontaneously formed small cell aggregates, and the polarized cells migrated toward these preexisting cell aggregates and became part of them (Fig. 11B; Movie S8). The small cell aggregates could be acting as aggregation centers by secreting chemoattractants and attracting

FIG 9 Legend (Continued)
moving randomly, as shown by the red tracks. (C) These changes could be seen in the circularity and aspect ratio. As adenosine was added to the cells, the aspect ratio started decreasing and circularity started increasing, since cells lost polarity. Later, the formation of multiple protrusions decreased the circularity and slightly increased the aspect ratio. (D) Adenosine binding activates frontness and produces multiple leading edges, causing the cell to move in multiple directions. (E) Ptx binding activates backness, which prevents lateral protrusions and confines the front to a single position so that the cell moves in a single direction. (F) Comparison of motility using *E. invadens* migratory tracks showed that the movement in growth medium contained patterns of both pentoxifylline- and adenosine-induced motility. Scale bar shows 100 μm.

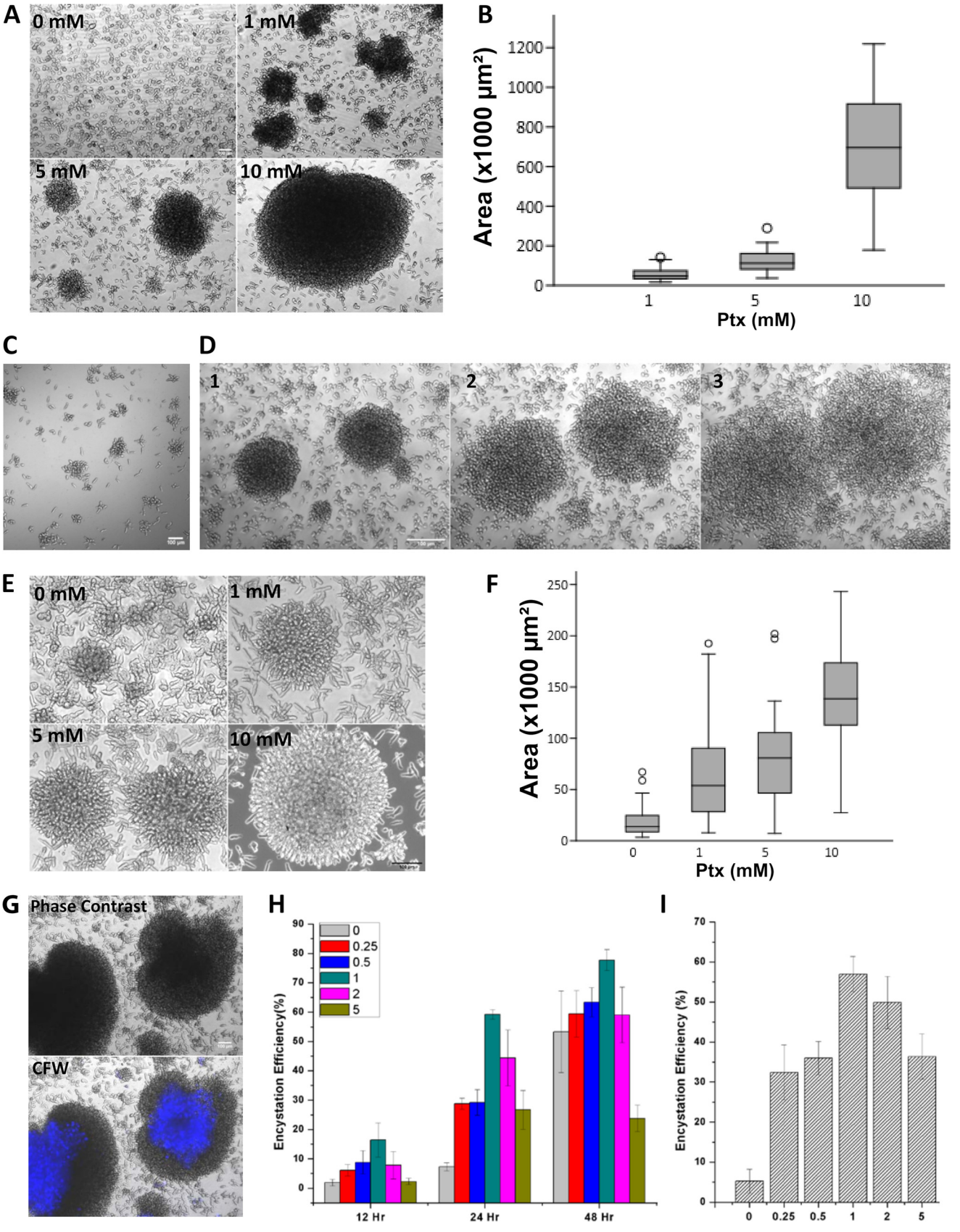

FIG 10 Stable bleb-driven morphology of *E. invadens* is aggregation competent. (A) In *E. invadens*, Ptx dose dependently induced cell aggregates in growth medium. (B) Box plots showing the cell aggregate size at 24 h in response to different Ptx concentrations, measured from its cross-sectional area. Data are

(Continued on next page)

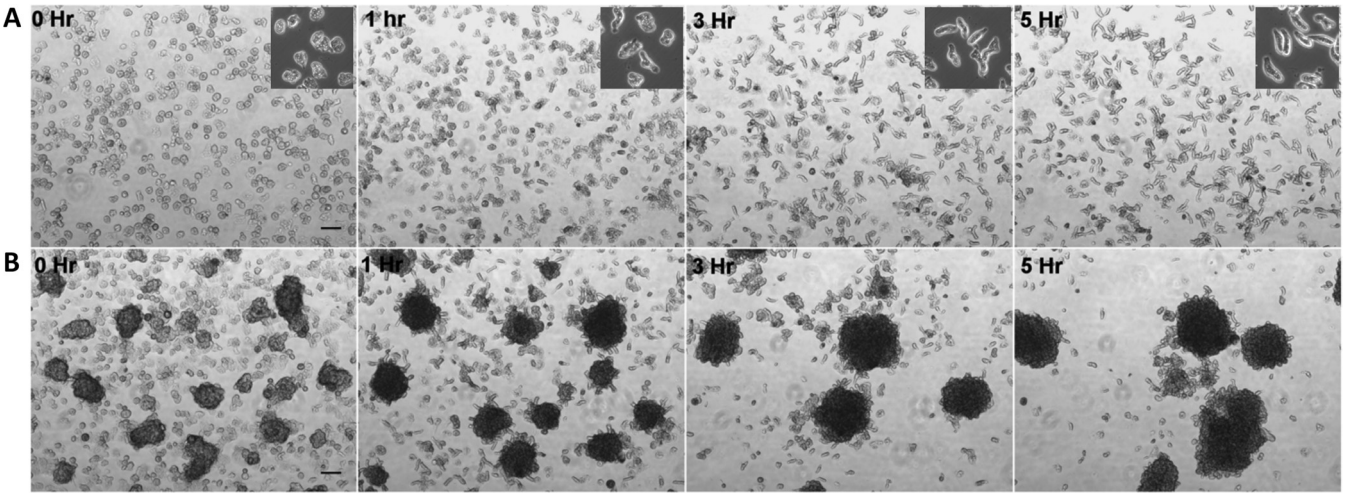

FIG 11 Stable bleb-driven form mediates cell aggregation during encystation. (A) When the growth medium was replaced with encystation medium, the trophozoites became polarized and highly motile. (B) In a confluent culture containing spontaneously formed small cell aggregates, the polarized motile cells moved toward the small aggregates, which acted as aggregation centers. Thus, the polarized morphology mediated the cell aggregation during early encystation. See also Movies S7 and S8. Scale bars show 100 μm.

the rest of the cells toward them. These observations clearly show that the cell aggregation during encystation is mediated by the directional migration of the stable bleb-driven polarized cells.

Purine nucleotides inhibit the cell polarity in *E. invadens*, preventing cell aggregation and encystation. Since adenosine and its antagonist Ptx were involved in controlling *Entamoeba* morphology, the effects of purine molecules on cell polarity, aggregation, and encystation were studied. Adenosine inhibited cell polarization and thus prevented Ptx-mediated cell aggregation in growth medium (Fig. 12A) and encystation medium (Fig. 12B) and also dose dependently reduced cyst formation (Fig. 12C). Also, uniformly added ATP (0.1 to 1.0 mM) led to an instantaneous loss of polarization of the stable bleb morphology (Fig. 12D), and a similar effect was seen with ADP and AMP. Actin localization with rhodamine-phalloidin following ATP treatment showed the formation of phagocytic and pinocytic invaginations in *E. invadens* cells, indicating their reversal to the unpolarized state (Fig. 12E). The addition of purine nucleotides like ATP, ADP, and AMP prevented and reversed the cell aggregation observed in both growth medium (Fig. 12F; Movie S9) and encystation medium (Fig. 12G; Movie S9). Unlike the instantaneous galactose-mediated disaggregation, ATP addition caused the cells to lose polarity and aggregation competency, and the cells slowly came out of aggregates and attached themselves to the substratum. Thus, purine nucleotides inhibited encystation by preventing the formation of stable bleb-driven monopodial morphology.

DISCUSSION

Treatment with millimolar concentrations of methylxanthines broke the cell symmetry in *Entamoeba* and produced an elongated polarized phenotype. The polarized morphology was monopodial, as it showed a single, round leading edge and a narrow

FIG 10 Legend (Continued)
presented as box plots, showing 25 to 75% quartiles as boxes, median values as horizontal lines inside the boxes, and outlier values as circles. (C) A concentration of 10 mM Ptx induced cell aggregation even at low cell densities (10^3 cells/ml), showing the aggregation competency of the stable bleb-driven morphology. (D) Galactose (10 mM) caused disaggregation of Ptx-induced cell aggregates, indicating they are also galactose ligand mediated, like the cell aggregates in encystation medium. (E) The addition of Ptx to the encystation culture was found to enhance cell aggregation in the early hours. (F) The cell aggregate sizes in response to different Ptx concentrations after 3 h in the encystation culture, measured from their cross-sectional areas. Data are presented as box plots, showing 25 to 75% quartiles as boxes, median values as horizontal lines inside the boxes, and outlier values as circles. (G) Cysts were formed inside the Ptx-induced aggregates within 24 h, as shown by calcofluor white (CFW) staining (blue). (H) Time courses of encystation after treatment with different Ptx concentrations showed that up to 1 mM, Ptx increased encystation, but higher concentrations were inhibitory. (I) In serum-deficient encystation medium, Ptx increased cyst formation up to 1 mM. Scale bars show 100 μm.

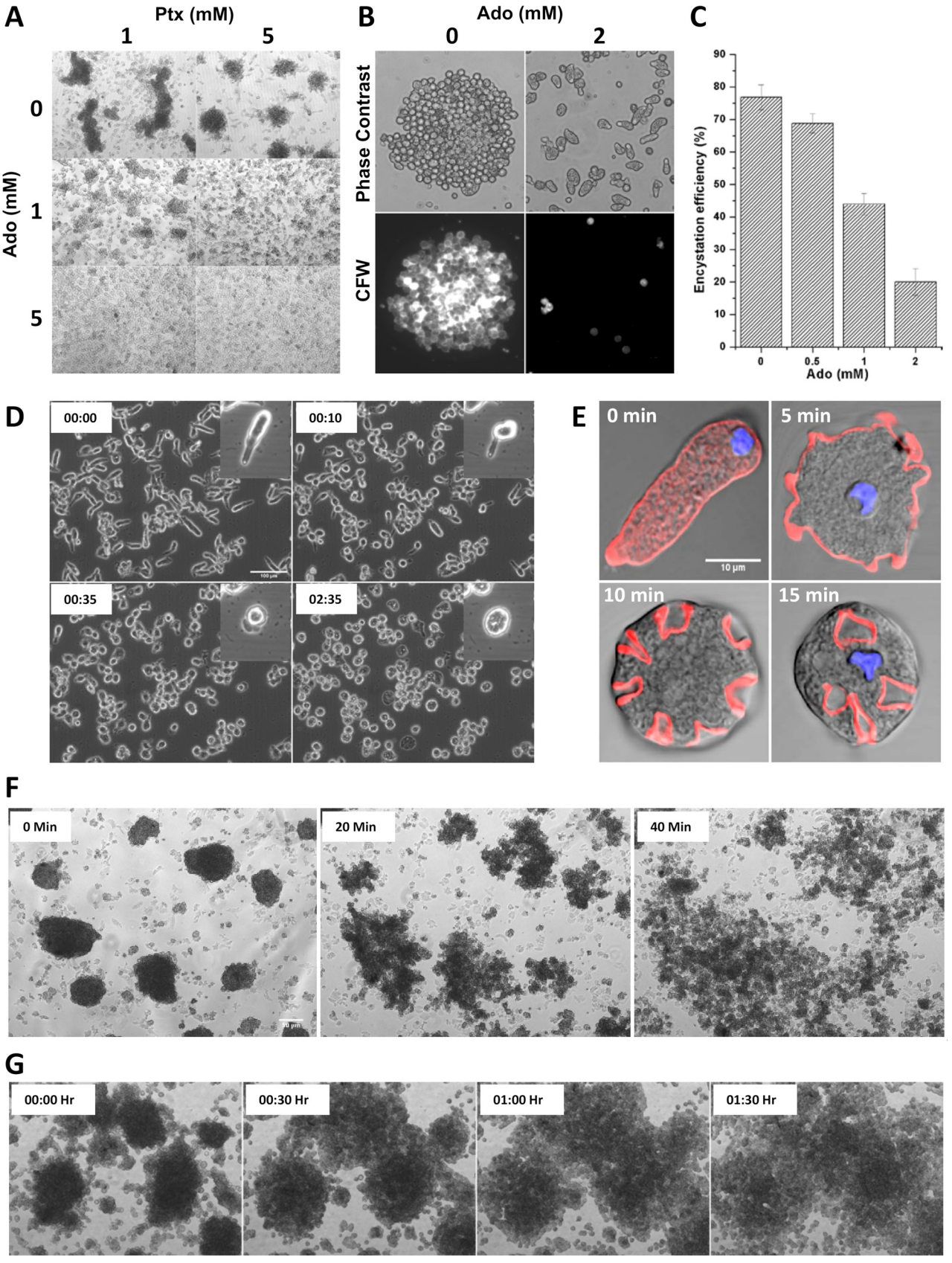

FIG 12 Purine nucleotides inhibit encystation in *E. invadens* by preventing cell polarization and aggregation. (A) Adenosine (Ado) inhibited Ptx-induced cell aggregation in growth medium. (B) The presence of 2 mM adenosine in the encystation culture also prevented cell aggregation. (C) Adenosine dose

(Continued on next page)

trailing uroid and no lateral protrusions. Its cytoplasm was divided into a central fluid endoplasm, surrounded by a stationary gelated ectoplasm. Tracking of intracellular particles showed that the endoplasm moved in the travelling direction and was congealed into ectoplasm at the front, and at the rear, the ectoplasm was reconverted into the endoplasm. This cyclic sol-gel conversion caused a rearward movement of the cell surface relative to the leading edge, propelling the cell forward. Cross-linking cell surface particles with concanavalin A resulted in their capping at the rear end of the polarized *Entamoeba* cell, and this can be taken as evidence for such a backward flow of the cell surface. In migrating *Dictyostelium*, it has been shown that the membrane moves backward at speeds similar to that of cell migration (41). Retrograde flow of cell membranes has also been shown to drive adhesion-independent amoeboid cell migration (42). At the rear, the membrane is removed by endocytosis and trafficked to the front to replenish the anterior membrane (42, 43). Such an intracellular anterograde transport of the membrane vesicles was visible in the polarized form of *Entamoeba* cells as a fluorescing flow through the endoplasm. Thus, the rearward movement of the cell surface powered by the reversible sol-gel conversion of the cytoplasm propelled the polarized monopodial form of *Entamoeba*.

A single leading edge that was round in shape and deficient in actin but occasionally contained actin scars indicated that the polarized morphology was driven by a stable bleb (8, 18, 19). A bleb is formed when the intracellular pressure causes depolymerization of the cortical actin cytoskeleton, which detaches and pushes the membrane forward. The expansion of a bleb requires a membrane source, since the plasma membrane can be stretched by 2% to 3% before its rupture. The new membrane can be provided by the exocytosis of membrane (5) or by the unfolding of membrane invaginations (44). In the polarized *Entamoeba* cell, the continuous bleb expansion was supported by a membrane flow from the uroid to the front. The efflux of the endoplasmic sol into the inflated bleb and simultaneous retraction of the rear resulted in the forward translocation of the cell.

In the Ptx-induced polarized form, new blebs were generated only from the preexisting leading edge rather than in different directions around the cell, which altered the motility pattern from slow and random to directionally persistent and fast. Ptx was chemokinetic in *Entamoeba*, as it initiated the cell motility without dictating the direction of migration, but Ptx also enhanced the chemotaxis. In a polarized cell, the leading edge is more sensitive to chemoattractants than the sides or trailing edge. This localized sensitivity orients the leading edge toward a chemoattractant source, resulting in faster directional movement (45). In *Dictyostelium*, blebbing is induced by cyclic AMP, indicating the relationship between blebbing and chemotaxis signaling (46). Also, the blebbing cells of *Dictyostelium* are reported to be strongly chemotactic (8, 47). Thus, the front-rear polarity and the bleb-driven motility could be the reason for the increase in the chemotactic potential of the Ptx-induced morphology.

Following Ptx treatment, the adherent unpolarized trophozoites of *Entamoeba* formed the adherent lamellipodial stage, followed by adherent bleb-driven intermediate phenotypes and, finally, the nonadherent stable bleb-driven form. The type of cell protrusion is reported to depend on the substrate adhesion, as adhesive substrates caused lamellipodium formation and nonadhesive substrates, bleb-based protrusions (48). The reverse process was seen in *Entamoeba*: as blebbing became prominent, the cell adhesion reduced. Thus, like the mesenchymal amoeboid transition (7, 9), Ptx switched the slow, adherent, and unpolarized trophozoites to fast, highly chemotactic,

FIG 12 Legend (Continued)
dependently reduced encystation efficiency. (D) In the presence of ATP (100 μM), polarized cells that formed in response to 0.5 to 1 mM pentoxifylline or stress (starvation, heat, or oxidative stress) lost the cell polarity. ATP had no effect on polarity in the presence of 5 to 10 mM Ptx. Scale bar shows 100 μm. Time in seconds is shown. (E) Actin localization following ATP treatment showed the appearance of features of unpolarized cells, such as phagocytic and pinocytic invaginations. Scale bar shows 10 μm. (F) The addition of 0.5 mM ATP to confluent growth culture caused dispersion of cell aggregates. Scale bar shows 100 μm. (G) The presence of ATP (0.5 mM) in encystation medium also prevented the cell aggregation observed during *in vitro* encystation. See also Movie S9.

nonadherent, and polarized stable bleb-driven cells. These observations show that *Entamoeba* organisms possess different migration modes and can switch them. F-actin based adhesion structures disappeared during the cell polarization, but the stable bleb morphologies were highly motile under confinement. The velocity of stable bleb-driven *Entamoeba* cells nearly doubled in a confined environment, such as under an agarose layer. The adhesion-deficient cells showed normal locomotion under confinement, using traction from opposite surfaces by a movement called "chimneying" (34). Stable bleb morphologies of cancer and progenitor cells also have been shown to be highly motile in confinement (18, 19). Also, under agarose, stable bleb-driven *E. invadens* cells moved collectively, which was not observed under the medium, as the ability of cells to stream depended on the quantity of fluid medium due to the dilution of signaling molecules (36). Thus, *E. invadens* may be generating a chemoattractant gradient around the cell, which attracts and aligns other cells in a head-to-tail fashion (49), but such alignment was not observed in *E. histolytica*.

The formation of multiple leading edges caused by exogenous adenosine indicates it could be activating frontness signals in *Entamoeba*. Pentoxifylline inhibited lateral protrusions and confined the leading edge to one point, indicating the activation of backness signals. The cell polarity has been shown to be established and maintained by the local mutual inhibition between frontness signals and backness signals (50). Thus, adenosine could be promoting a strong frontness in *Entamoeba*, whereas pentoxifylline is promoting a strong backness. In *Dictyostelium*, attractants and repellents initiated cell polarization and migration in "front-driven" and "rear-driven" modes, respectively (51), and our observations indicate *Entamoeba* also has such a guidance mechanism. The adenosine receptors are reported to regulate the cell motility during chemotaxis by autocrine purinergic signaling (52). According to the purinergic signaling system (53), chemotactic signals induce a localized release of ATP at the leading edge, followed by hydrolysis of ATP to adenosine, which then acts on the adenosine receptors to promote migration. The purinergic signaling is present in all kingdoms of life, and extracellular purines like ATP and adenosine have been shown to elicit multiple responses in many protozoans (54). Though the *Entamoeba* purine receptors are not yet identified, the present work indicates the possible existence of purinergic signaling in *Entamoeba*. This was further confirmed when the presence of extracellular adenine nucleotides inhibited the polarity of the bleb-driven form and prevented cell aggregation and encystation. Animal cells contain 5 to 10 mM ATP in their cytosol, and the tissue damage by *Entamoeba* may cause leakage of ATP from damaged cells. Such accumulation of purine nucleotides in the surroundings of *Entamoeba* cells, especially in tissue lesions formed during invasive amoebiasis, may have some effect on the invasiveness and the life cycle of *Entamoeba*, but further research is required to confirm this.

During the purinergic control of cell motility, the endogenous ATP released through exocytosis has been shown to control the chemotaxis of microglial (55) and cancer cell migration (56). During the early hours of encystation, ATP and other nucleotides transiently increased and then decreased (57). This decrease may be due to exocytosis, and the released ATP may be initiating purinergic signaling during early encystation. As in other amoebas, multicellular aggregate formation took place during the early hours of encystation in *E. invadens*, and like that of other amoebas, it could be mediated by chemotaxis. An important property of the stable bleb-driven polarized phenotype was its ability to form galactose ligand-mediated multicellular aggregates similar to those found in the encystation medium. Ptx dose dependently increased the cell aggregation in both growth and encystation medium, but it increased the encystation efficiency only up to 1 mM concentration and thereafter reduced cyst formation. While cell aggregation is indispensable for encystation, cysts were not formed in every cell aggregate, like the Ptx-induced cell aggregates in the growth medium. Ptx up to 1 mM concentration significantly enhanced the encystation efficiency at early time points (12 h and 24 h), and so the effect of Ptx on encystation may have been due to the formation of the polarized phenotype, which in turn mediated the cell aggregation. At

concentrations above 1 mM, Ptx may be having off-target effects on the encystation pathway, but the mechanism of inhibition is not clear.

Live-cell video microscopy revealed that encystation stimuli induced the formation of the stable bleb-driven polarized form, which actively moved toward small cell clusters, forming the multicellular structures. Here, the small cell aggregates may be acting as aggregation centers secreting chemoattractants. Spontaneous cell aggregation took place in a confluent growth culture, and when two strains of *E. invadens* were kept together, cells aggregated only with members of their strain (58), indicating the cell aggregation in *Entamoeba* may be mediated by chemotaxis. While such aggregations took place slowly, Ptx treatment and encystation stimuli made the process faster, because polarized cells are much more efficient in chemotaxis. Ptx also induced cell aggregation in *E. histolytica* but required high cell density ($>10^6$ cells/ml) and high Ptx concentration (>10 mM), and these cell aggregates were short lived. Also, the polarized cells of *E. invadens* were more chemotactic than those of *E. histolytica*. These differences in the chemotactic and aggregation potential could be the reasons the *E. invadens* cells readily aggregated and encysted *in vitro* in response to nutrient and osmotic stress but the *E. histolytica* cells did not. Apart from the Ptx and encystation stimuli, most stress conditions, such as starvation, oxidative stress, and heat stress, induced the stable bleb morphology in *E. invadens*. In *E. histolytica*, such morphology was reported only under a chemoattractant gradient like that of TNF (59). We also observed that when exposed to continuous oxidative or heat stresses, both *E. histolytica* and *E. invadens* trophozoites formed large numbers of elongated cells with a fluid-filled hyaline cap at the leading edge (Fig. S8A and B). The actin localization of these cells was similar to that of the stable bleb cells (Fig. S8C). Though this morphological form was similar to that of the stable bleb cells, their importance in the *Entamoeba* life cycle is not yet evident.

The polarization and motility of *Entamoeba* are required for invasive amoebiasis (9, 10), and chemotactic and chemokinetic stimulations by molecules like TNF are reported to have an important role in invasive amoebiasis (12). Migration of *E. histolytica* cells inside the extracellular matrix (ECM) of low collagen density was independent of protease activity and depended on the deformation of cell shape (60). The low substrate-cell adhesion, extensive blebbing, and high velocity of locomotion, especially under confinement, could facilitate the squeezing of the stable bleb cells through the pores in the ECM, resulting in a "pathfinding" amoeboid-type invasion (7). Stable bleb-driven forms of *Entamoeba*, cancer cells, and progenitor cells share similar morphological and motile features, such as cell shape, high speed, low adhesion, and actomyosin distribution, and such bleb-driven motility is suspected to be the primitive form of locomotion present in eukaryotes (18). Also, *E. invadens* and *E. histolytica* may be used as a model system for studying bleb-based amoeboid migration and other aspects of cell movement, as their morphology and motility *in vitro* can be easily controlled.

MATERIALS AND METHODS

Cells and reagents. *Entamoeba invadens* (strain IP-1) and *Entamoeba histolytica* (strain HM1-IMSS) cells were cultured in TYI-S-33 medium (61) completed with 10% heat-inactivated adult bovine serum (HiMedia), 3% Diamond vitamin mix, penicillin, and streptomycin at 25°C and 37°C, respectively. LG100 was prepared by making TYI-S-33 medium without glucose (100% LG), and the encystation medium LG47 was prepared by diluting LG100 2.12 times (47% LG) supplemented with 5% adult bovine serum, vitamin mix, and antibiotics. Pentoxifylline, caffeine, Texas red-concanavalin A, DAPI (4′,6-diamidino-2-phenylindole), adenosine, ATP, fluorescein diacetate, and calcofluor white were purchased from Sigma-Aldrich. Rhodamine-conjugated phalloidin and CellMask orange were purchased from Molecular Probes, Invitrogen, USA. Transwell inserts with 8-μm pores were obtained from SPL Life Sciences Co., Ltd., Republic of Korea.

Microscopy. Time-lapse video microscopy images and phase-contrast images were taken using an Olympus IX51 inverted light microscope with a camera attachment and photoediting software (Image Pro Discovery). An Olympus FV1000 confocal microscope with Fluoview software was used for fluorescence imaging. The raw images were processed using ImageJ (http://rsbweb.nih.gov/ij/) containing appropriate plugins.

Calculation of cell shape descriptors. The changes in the morphology were quantitatively defined using shape descriptors aspect ratio and circularity. The values for aspect ratio and circularity were calculated from the images using ImageJ. Aspect ratio is the ratio of the length of the major axis to the

minor axis for an ellipse. For spherical morphology, the aspect ratio = 1, whereas for an elongated morphology, the aspect ratio is >1. Circularity is calculated as $4\pi \times$ (area)/(perimeter)^2. Values of 1.0 indicate a perfect circle, and lower values indicate the formation of protrusions. Unpolarized stationary cells showed high circularity, and low circularity is a trait of polarized migrating cells. The measurements were taken a minimum of three times independently from an average of 30 cells for each data point.

Actin staining. Morphological changes in *Entamoeba* cells were analyzed by actin staining with rhodamine-phalloidin. Clean coverslips were placed in 35-mm cell culture plates, and trophozoites at an appropriate cell density were seeded and allowed to adhere. After the addition of Ptx, adenosine, or ATP, the cells were fixed at different time points using 3% paraformaldehyde prewarmed at room temperature for 30 min and then permeabilized with 0.2% (vol/vol) Triton X-100 in phosphate-buffered saline (PBS) for 5 min. The actin cytoskeleton was then visualized by staining the permeabilized cells with rhodamine-conjugated phalloidin after blocking the permeabilized cells with 2% (wt/vol) bovine serum albumin (BSA).

Cell membrane staining. To study plasma membrane dynamics during motility, polarized and unpolarized cells grown on coverslips were treated with CellMask Orange (Invitrogen) at 1:1,000 dilution. After 1 min of incubation, the excess dye was removed by washing with PBS, and the cell movement was recorded with the confocal microscope.

Cap induction in *Entamoeba*. To find the capping of cell surface proteins, trophozoites grown on glass coverslips were incubated with Texas red-concanavalin A (50 μg/ml) in the absence or presence of Ptx for 5 min. After the cells were washed with PBS, they were fixed and observed under the microscope.

Analysis of leading-edge behavior. Images were acquired by time-lapse microscopy, and the changes in the cell morphology, protrusion formation, and leading-edge dynamics were analyzed by detecting the cell outline changes and generating kymographs. ImageJ was used to extract cell outlines from phase-contrast images. For this, Sobel edge detector was first applied to the images. A threshold was then applied to get a binary gradient mask containing the cell. It was then dilated, and the holes in the interior of the cell were filled. The image was then smoothed, and the cell outline was extracted. After the outline from each image of the time-lapse movie was color coded, they were overlaid. To generate a kymograph, a segmented line was drawn along the migratory trajectory of the cell. Then, using ImageJ software and the Multiple Kymograph plug-in, the space-time graph was plotted with the *x* axis representing distance and the *y* axis time.

Analysis of cell motility and tracking of particles. Time-lapse video microscopy was performed using an Olympus IX51 inverted microscope with a camera attachment and photo-editing software (Image Pro Discovery). Images were taken at appropriate intervals to produce a time-lapse movie. Using the ImageJ software with plugins Manual Tracking and MTrackJ, the position of cells or intracellular particles at different time points were identified from the time lapse. An average of 20 to 30 cells was tracked during the experiment, and each experiment was repeated at least three times. From the positions of each cell, the migratory tracks were visualized using the Chemotaxis and Migration Tool (Ibidi), which was then used to calculate the migration velocity and the directness (*D*). The velocity of each cell was calculated as the total distance covered divided by time, and the average velocity for each experiment was calculated. Directness is the measure of a cell's tendency to travel in a straight line. It is calculated by dividing the displacement by the distance. *D* is the average of all values of directness for all cells. A directness of $D = 1$ indicates a straight-line migration from start to endpoint, while $D << 1$ indicates random motility.

Transwell migration assay. Transwell migration assays (Boyden chamber assay) were conducted to measure the chemokinesis and chemotaxis. For this, transwell inserts with 8-μm-pore-size polycarbonate membranes and 24-well cell culture plates were used. To measure chemotaxis, complete TYI-S-33 medium or TYI-S-33 medium containing chemoattractant (0.5 ml) was placed in the bottom chamber. Trophozoites at a concentration of 1.0×10^5 cells/ml in incomplete TYI medium were then added to the upper well chamber. To test chemokinesis, the chemical was added separately to the top and bottom chambers. The 24-well plates were then sealed with parafilm and placed in an anaerobic bag for 3 h. Trophozoites that had migrated to the lower chamber were detached from the culture plate by keeping the plate on ice, harvested, and counted using a hemocytometer. The extent of migration was expressed as the fold change of the number of migrated cells relative to the number of control cells. The experiments were carried out in triplicates and were repeated at least three times.

Under-agarose assay. For the under-agarose assay, 0.7% agarose dissolved in TYI medium without glucose (LG100) was poured into 100-mm plastic petri dishes and allowed to solidify. A 2-mm-wide trough was made at the center of the petri dish. *Entamoeba* cells were harvested, adjusted to 10^5 amoebae/ml in LG100, and added to the trough. Plates were maintained at 25°C and 37°C for *E. invadens* and *E. histolytica*, respectively. Once the cells moved under the agarose gels, their movements were recorded with time-lapse microscopy. The assay was repeated in the presence and absence of Ptx a minimum of three times, with an average of 20 to 30 cells being tracked during each experiment, and the motility characteristics were analyzed as described above.

Cell adhesion assay. *E. histolytica* and *E. invadens* cells were plated in 24-well multiwell plates and treated with different concentrations of pentoxifylline. After 12 h of incubation, the wells were washed with PBS three times to remove nonadherent cells. Remaining adherent cells in the wells were then counted in randomly selected fields using a microscope and plotted against Ptx concentrations. The number of adherent cells in the untreated control was arbitrarily set to 100%, and the values from Ptx treatment are reported as percentages of this value. The experiments were repeated a minimum of three times, and at least 100 cells were counted for each value.

Encystation. To prepare the encystation medium (LG47), TYI-S-33 medium without glucose (100% LG) was prepared and diluted 2.12 times and then completed with 5% adult bovine serum, 1.5% vitamin mix, and penicillin and streptomycin. Mid-log-phase trophozoites were chilled on ice for 10 min to detach the cells from the culture tube wall and harvested by centrifugation at 500 × *g* for 5 min at 4°C. These cells were washed 3 times with encystation medium (LG47), adjusted to 5×10^5 trophozoites per ml, and incubated at 25°C. Serum-deficient encystation medium did not contain the usual 5% adult bovine serum, and it was used to find the effect of Ptx on aggregation and cyst formation under serumless conditions. To find the response of *E. invadens* to encystation medium by time-lapse microscopy, cells were grown in tissue culture plates, and TYI-S-33 medium was replaced with the LG47 medium. *E. invadens* cultures below confluence and confluent cultures with small cell aggregates were used. The formation of cysts inside the cell aggregates was confirmed by adding calcofluor white to the encystation medium and observing under the fluorescence microscope. The encystation efficiency was calculated from the percentage of detergent-resistant (0.1% Sarkosyl) and chitin-positive cysts after staining with calcofluor white (25 μM). Maturation of cysts was confirmed by visualizing the three features of a mature *Entamoeba* cyst, which are a chitin wall, four nuclei, and a chromatoid body, by staining with calcofluor white, DAPI, and toluidine blue, respectively. Each encystation experiment was repeated a minimum of three times, and at least 60 cells were counted to calculate encystation efficiency at each time point.

Cell viability determination. Cells were treated with 10 mM Ptx for 48 h and then stained with PBS containing 10 μg/ml of fluorescein diacetate. After 5 min of incubation at room temperature, cells were washed with PBS and then observed under a fluorescence microscope for the green fluorescence produced by live cells.

Cell aggregate size calculation. *E. invadens* cells were grown in 24-well tissue culture plates, and Ptx was added at different concentrations to induce cell aggregation. To find the enhancement of cell aggregation in encystation medium by Ptx, *E. invadens* cells at a cell density of 5×10^5 cells/ml were resuspended in 47% LG and transferred to a 24-well tissue culture-treated plate. After imaging a minimum of 60 cell aggregates for each condition at ×4 magnification, the cross-sectional area of each aggregate was measured using ImageJ. Data are presented in the figures as box plots.

Statistical analysis. Quantitative data are presented as the mean value ± standard deviation of a minimum of three independent experiments. Comparison between groups was performed with analysis of variance (ANOVA), and the significance of the experimental data was estimated using Student's *t* test. The results were considered statistically significant only if P was <0.05. Statistical significance is represented in the figures as follows: *, $P < 0.05$; **, $P < 0.01$; ***, $P < 0.001$; and ns, not significant.

SUPPLEMENTAL MATERIAL

Supplemental material is available online only.

SUPPLEMENTAL FILE 1, PDF file, 1.6 MB.

SUPPLEMENTAL FILE 2, MP4 file, 14.9 MB.

SUPPLEMENTAL FILE 3, MP4 file, 15.3 MB.

SUPPLEMENTAL FILE 4, AVI file, 0.3 MB.

SUPPLEMENTAL FILE 5, MP4 file, 6.5 MB.

SUPPLEMENTAL FILE 6, MP4 file, 6 MB.

SUPPLEMENTAL FILE 7, MP4 file, 2.9 MB.

SUPPLEMENTAL FILE 8, MP4 file, 16.4 MB.

SUPPLEMENTAL FILE 9, MP4 file, 14.3 MB.

SUPPLEMENTAL FILE 10, MP4 file, 2.2 MB.

ACKNOWLEDGMENTS

S.K.G. would like to acknowledge DBT and MHRD, Government of India, for financial support. D.K. is the recipient of a senior research fellowship from the Indian Council of Medical Research, India.

We thank FIST, DST, Government of India for support of the confocal facility.

We declare no competing or financial interests.

D.K. and S.K.G. designed the research; D.K. performed the research; and D.K. and S.K.G. wrote the paper.

REFERENCES

1. Petrie RJ, Doyle AD, Yamada KM. 2009. Random versus directionally persistent cell migration. Nat Rev Mol Cell Biol 10:538–549. https://doi.org/10.1038/nrm2729.
2. Pankov R, Endo Y, Even-Ram S, Araki M, Clark K, Cukierman E, Matsumoto K, Yamada KM. 2005. A Rac switch regulates random versus directionally persistent cell migration. J Cell Biol 170:793–802. https://doi.org/10.1083/jcb.200503152.
3. Iglesias PA, Devreotes PN. 2008. Navigating through models of chemotaxis. Curr Opin Cell Biol 20:35–40. https://doi.org/10.1016/j.ceb.2007.11.011.

4. Cai H, Devreotes PN. 2011. Moving in the right direction: how eukaryotic cells migrate along chemical gradients. Semin Cell Dev Biol 22:834–841. https://doi.org/10.1016/j.semcdb.2011.07.020.
5. Charras GT, Coughlin M, Mitchison TJ, Mahadevan L. 2008. Life and times of a cellular bleb. Biophys J 94:1836–1853. https://doi.org/10.1529/biophysj.107.113605.
6. Blaser H, Reichman-Fried M, Castanon I, Dumstrei K, Marlow FL, Kawakami K, Solnica-Krezel L, Heisenberg CP, Raz E. 2006. Migration of zebrafish primordial germ cells: a role for myosin contraction and cytoplasmic flow. Dev Cell 11:613–627. https://doi.org/10.1016/j.devcel.2006.09.023.
7. Panková K, Rösel D, Novotný M, Brábek J. 2010. The molecular mechanisms of transition between mesenchymal and amoeboid invasiveness in tumor cells. Cell Mol Life Sci 67:63–71. https://doi.org/10.1007/s00018-009-0132-1.
8. Zatulovskiy E, Tyson R, Bretschneider T, Kay RR. 2014. Bleb-driven chemotaxis of Dictyostelium cells. J Cell Biol 204:1027–1044. https://doi.org/10.1083/jcb.201306147.
9. Dufour AC, Olivo-Marin JC, Guillen N. 2015. Amoeboid movement in protozoan pathogens. Semin Cell Dev Biol 46:128–134. https://doi.org/10.1016/j.semcdb.2015.10.010.
10. Aguilar-Rojas A, Olivo-Marin JC, Guillen N. 2016. The motility of *Entamoeba histolytica*: finding ways to understand intestinal amoebiasis. Curr Opin Microbiol 34:24–30. https://doi.org/10.1016/j.mib.2016.07.016.
11. Bailey GB, Leitch GJ, Day DB. 1985. Chemotaxis by *Entamoeba histolytica*. J Protozool 32:341–346. https://doi.org/10.1111/j.1550-7408.1985.tb03063.x.
12. Blazquez S, Zimmer C, Guigon G, Olivo-Marin J-C, Guillén N, Labruyère E. 2006. Human tumor necrosis factor is a chemoattractant for the parasite *Entamoeba histolytica*. Infect Immun 74:1407–1411. https://doi.org/10.1128/IAI.74.2.1407-1411.2006.
13. Silvestre A, Plaze A, Berthon P, Thibeaux R, Guillen N, Labruyère E. 2015. In *Entamoeba histolytica*, a BspA family protein is required for chemotaxis toward tumour necrosis factor. Microb Cell 2:235–246. https://doi.org/10.15698/mic2015.07.214.
14. Zaki M, Andrew N, Insall RM. 2006. *Entamoeba histolytica* cell movement: a central role for self-generated chemokines and chemorepellents. Proc Natl Acad Sci U S A 103:18751–18756. https://doi.org/10.1073/pnas.0605437103.
15. Ghosh SK, Van Dellen KL, Chatterjee A, Dey T, Haque R, Robbins PW, Samuelson J. 2010. The Jacob2 lectin of the *Entamoeba histolytica* cyst wall binds chitin and is polymorphic. PLoS Negl Trop Dis 4:e750. https://doi.org/10.1371/journal.pntd.0000750.
16. Du Q, Kawabe Y, Schilde C, Chen ZH, Schaap P. 2015. The evolution of aggregative multicellularity and cell-cell communication in the Dictyostelia. J Mol Biol 427:3722–3733. https://doi.org/10.1016/j.jmb.2015.08.008.
17. Maugis B, Brugués J, Nassoy P, Guillen N, Sens P, Amblard F. 2010. Dynamic instability of the intracellular pressure drives bleb-based motility. J Cell Sci 123:3884–3892. https://doi.org/10.1242/jcs.065672.
18. Liu YJ, Le Berre M, Lautenschlaeger F, Maiuri P, Callan-Jones A, Heuzé M, Takaki T, Voituriez R, Piel M. 2015. Confinement and low adhesion induce fast amoeboid migration of slow mesenchymal cells. Cell 160:659–672. https://doi.org/10.1016/j.cell.2015.01.007.
19. Ruprecht V, Wieser S, Callan-Jones A, Smutny M, Morita H, Sako K, Barone V, Ritsch-Marte M, Sixt M, Voituriez R, Heisenberg CP. 2015. Cortical contractility triggers a stochastic switch to fast amoeboid cell motility. Cell 160:673–685. https://doi.org/10.1016/j.cell.2015.01.008.
20. Logue JS, Cartagena-Rivera AX, Baird MA, Davidson MW, Chadwick RS, Waterman CM. 2015. Erk regulation of actin capping and bundling by Eps8 promotes cortex tension and leader bleb-based migration. Elife 4:e08314. https://doi.org/10.7554/eLife.08314.
21. Yoshida K, Inouye K. 2001. Myosin II-dependent cylindrical protrusions induced by quinine in *Dictyostelium*: antagonizing effects of actin polymerization at the leading edge. J Cell Sci 114:2155–2165.
22. Bergert M, Erzberger A, Desai RA, Aspalter IM, Oates AC, Charras G, Salbreux G, Paluch EK. 2015. Force transmission during adhesion-independent migration. Nat Cell Biol 17:524–529. https://doi.org/10.1038/ncb3134.
23. Coppi A, Merali S, Eichinger D. 2002. The enteric parasite *Entamoeba* uses an autocrine catecholamine system during differentiation into the infectious cyst stage. J Biol Chem 277:8083–8090. https://doi.org/10.1074/jbc.M111895200.
24. Schaap P. 2011. Evolution of developmental cyclic adenosine monophosphate signaling in the Dictyostelia from an amoebozoan stress response. Dev Growth Differ 53:452–462. https://doi.org/10.1111/j.1440-169X.2011.01263.x.
25. Brenner M, Thoms SD. 1984. Caffeine blocks activation of cyclic AMP synthesis in *Dictyostelium discoideum*. Dev Biol 101:136–146. https://doi.org/10.1016/0012-1606(84)90124-6.
26. Lomakin AJ, Lee KC, Han SJ, Bui DA, Davidson M, Mogilner A, Danuser G. 2015. Competition for actin between two distinct F-actin networks defines a bistable switch for cell polarization. Nat Cell Biol 17:1435–1445. https://doi.org/10.1038/ncb3246.
27. Vayssié L, Vargas M, Weber C, Guillén N. 2004. Double-stranded RNA mediates homology-dependant gene silencing of γ-tubulin in the human parasite *Entamoeba histolytica*. Mol Biochem Parasitol 138:21–28. https://doi.org/10.1016/j.molbiopara.2004.07.005.
28. Zengel P, Nguyen-Hoang A, Schildhammer C, Zantl R, Kahl V, Horn E. 2011. μ-Slide chemotaxis: a new chamber for long-term chemotaxis studies. BMC Cell Biol 12:21. https://doi.org/10.1186/1471-2121-12-21.
29. Wang F, Van Brocklyn JR, Hobson JP, Movafagh S, Zukowska-Grojec Z, Milstien S, Spiegel S. 1999. Sphingosine 1-phosphate stimulates cell migration through a G(i)-coupled cell surface receptor. Potential involvement in angiogenesis. J Biol Chem 274:35343–35350. https://doi.org/10.1074/jbc.274.50.35343.
30. Frondorf K, Henkels KM, Frohman MA, Gomez-Cambronero J. 2010. Phosphatidic acid is a leukocyte chemoattractant that acts through S6 kinase signaling. J Biol Chem 285:15837–15847. https://doi.org/10.1074/jbc.M109.070524.
31. Bosgraaf L, Waijer A, Engel R, Visser AJ, Wessels D, Soll D, van Haastert PJ. 2005. RasGEF-containing proteins GbpC and GbpD have differential effects on cell polarity and chemotaxis in *Dictyostelium*. J Cell Sci 118:1899–1910. https://doi.org/10.1242/jcs.02317.
32. Fukui Y, Inoué S. 1997. Amoeboid movement anchored by eupodia, new actin-rich knobby feet in *Dictyostelium*. Cell Motil Cytoskeleton 36:339–354. https://doi.org/10.1002/(SICI)1097-0169(1997)36:4<339::AID-CM4>3.0.CO;2-0.
33. Uchida KSK, Yumura S. 2004. Dynamics of novel feet of *Dictyostelium* cells during migration. J Cell Sci 117:1443–1455. https://doi.org/10.1242/jcs.01015.
34. Malawista SE, De Chevance AB, Boxer LA. 2000. Random locomotion and chemotaxis of human blood polymorphonuclear leukocytes from a patient with leukocyte adhesion deficiency-1: normal displacement in close quarters via chimneying. Cell Motil Cytoskeleton 46:183–189. https://doi.org/10.1002/1097-0169(200007)46:3<183::AID-CM3>3.0.CO;2-2.
35. Krishnan D, Ghosh SK. 2018. Cellular events of multinucleated giant cells formation during the encystation of *Entamoeba invadens*. Front Cell Infect Microbiol 8:262. https://doi.org/10.3389/fcimb.2018.00262.
36. McCann CP, Kriebel PW, Parent CA, Losert W. 2010. Cell speed, persistence and information transmission during signal relay and collective migration. J Cell Sci 123:1724–1731. https://doi.org/10.1242/jcs.060137.
37. Sanchez L, Enea V, Eichinger D. 1994. Identification of a developmentally regulated transcript expressed during encystation of *Entamoeba invadens*. Mol Biochem Parasitol 67:125–135. https://doi.org/10.1016/0166-6851(94)90102-3.
38. Cho J, Eichinger D. 1998. *Crithidia fasciculata* induces encystation of *Entamoeba invadens* in a galactose-dependent manner. J Parasitol 84:705–710. https://doi.org/10.2307/3284574.
39. Coppi A, Eichinger D. 1999. Regulation of *Entamoeba invadens* encystation and gene expression with galactose and N-acetylglucosamine. Mol Biochem Parasitol 102:67–77. https://doi.org/10.1016/s0166-6851(99)00085-7.
40. Frisardi M, Ghosh SK, Field J, Van Dellen K, Rogers R, Robbins P, Samuelson J. 2000. The most abundant glycoprotein of amebic cyst walls (Jacob) is a lectin with five Cys-rich, chitin-binding domains. Infect Immun 68:4217–4224. https://doi.org/10.1128/iai.68.7.4217-4224.2000.
41. Tanaka M, Kikuchi T, Uno H, Okita K, Kitanishi-Yumura T, Yumura S. 2017. Turnover and flow of the cell membrane for cell migration. Sci Rep 7:1–3. https://doi.org/10.1038/s41598-017-13438-5.
42. O'Neill PR, Castillo-Badillo JA, Meshik X, Kalyanaraman V, Melgarejo K, Gautam N. 2018. Membrane flow drives an adhesion-independent amoeboid cell migration mode. Dev Cell 46:9–22.e4. https://doi.org/10.1016/j.devcel.2018.05.029.
43. Gras S, Jimenez-Ruiz E, Klinger CM, Schneider K, Klingl A, Lemgruber L, Meissner M. 2019. An endocytic-secretory cycle participates in *Toxoplasma gondii* in motility. PLoS Biol 17:e3000060. https://doi.org/10.1371/journal.pbio.3000060.

44. Goudarzi M, Tarbashevich K, Mildner K, Begemann I, Garcia J, Paksa A, Reichman-Fried M, Mahabaleshwar H, Blaser H, Hartwig J, Zeuschner D, Galic M, Bagnat M, Betz T, Raz E. 2017. Bleb expansion in migrating cells depends on supply of membrane from cell surface invaginations. Dev Cell 43:577–587.e5. https://doi.org/10.1016/j.devcel.2017.10.030.
45. Devreotes P, Janetopoulos C. 2003. Eukaryotic chemotaxis: distinctions between directional sensing and polarization. J Biol Chem 278:20445–20448. https://doi.org/10.1074/jbc.R300010200.
46. Langridge PD, Kay RR. 2006. Blebbing of *Dictyostelium* cells in response to chemoattractant. Exp Cell Res 312:2009–2017. https://doi.org/10.1016/j.yexcr.2006.03.007.
47. Yoshida K, Soldati T. 2006. Dissection of amoeboid movement into two mechanically distinct modes. J Cell Sci 119:3833–3844. https://doi.org/10.1242/jcs.03152.
48. Bergert M, Chandradoss SD, Desai RA, Paluch E. 2012. Cell mechanics control rapid transitions between blebs and lamellipodia during migration. Proc Natl Acad Sci U S A 109:14434–14439. https://doi.org/10.1073/pnas.1207968109.
49. Kriebel PW, Barr VA, Parent CA. 2003. Adenylyl cyclase localization regulates streaming during chemotaxis. Cell 112:549–560. https://doi.org/10.1016/s0092-8674(03)00081-3.
50. Xu J, Wang F, Van Keymeulen A, Herzmark P, Straight A, Kelly K, Takuwa Y, Sugimoto N, Mitchison T, Bourne HR. 2003. Divergent signals and cytoskeletal assemblies regulate self-organizing polarity in neutrophils. Cell 114:201–214. https://doi.org/10.1016/s0092-8674(03)00555-5.
51. Cramer LP, Kay RR, Zatulovskiy E. 2018. Repellent and attractant guidance cues initiate cell migration by distinct rear-driven and front-driven cytoskeletal mechanisms. Curr Biol 28:995–1004. https://doi.org/10.1016/j.cub.2018.02.024.
52. Ledderose C, Hefti MM, Chen Y, Bao Y, Seier T, Li L, Woehrle T, Zhang J, Junger WG. 2016. Adenosine arrests breast cancer cell motility by A3 receptor stimulation. Purinergic Signal 12:673–685. https://doi.org/10.1007/s11302-016-9531-6.
53. Chen Y, Corriden R, Inoue Y, Yip L, Hashiguchi N, Zinkernagel A, Nizet V, Insel PA, Junger WG. 2006. ATP release guides neutrophil chemotaxis via P2Y2 and A3 receptors. Science 314:1792–1795. https://doi.org/10.1126/science.1132559.
54. Burnstock G, Verkhratsky A. 2009. Evolutionary origins of the purinergic signalling system. Acta Physiol (Oxf) 195:415–447. https://doi.org/10.1111/j.1748-1716.2009.01957.x.
55. Dou Y, Wu HJ, Li HQ, Qin S, Wang YE, Li J, Lou HF, Chen Z, Li XM, Luo QM, Duan S. 2012. Microglial migration mediated by ATP-induced ATP release from lysosomes. Cell Res 22:1022–1033. https://doi.org/10.1038/cr.2012.10.
56. Takai E, Tsukimoto M, Harada H, Sawada K, Moriyama Y, Kojima S. 2012. Autocrine regulation of TGF-b1-induced cell migration by exocytosis of ATP and activation of P2 receptors in human lung cancer cells. J Cell Sci 125:5051–5060. https://doi.org/10.1242/jcs.104976.
57. Jeelani G, Sato D, Husain A, Escueta-de Cadiz A, Sugimoto M, Soga T, Suematsu M, Nozaki T. 2012. Metabolic profiling of the protozoan parasite *Entamoeba invadens* revealed activation of unpredicted pathway during encystation. PLoS One 7:e37740. https://doi.org/10.1371/journal.pone.0037740.
58. Espinosa A, Paz-Y-Miño CG. 2012. Discrimination, crypticity, and incipient taxa in *Entamoeba*. J Eukaryot Microbiol 59:105–110. https://doi.org/10.1111/j.1550-7408.2011.00606.x.
59. Blazquez S, Guigon G, Weber C, Syan S, Sismeiro O, Coppée JY, Labruyère E, Guillén N. 2008. Chemotaxis of *Entamoeba histolytica* towards the pro-inflammatory cytokine TNF is based on PI3K signalling, cytoskeleton reorganization and the galactose/N-acetylgalactosamine lectin activity. Cell Microbiol 10:1676–1686. https://doi.org/10.1111/j.1462-5822.2008.01158.x.
60. Thibeaux R, Dufour A, Roux P, Bernier M, Baglin AC, Frileux P, Olivo-Marin JC, Guillén N, Labruyère E. 2012. Newly visualized fibrillar collagen scaffolds dictate *Entamoeba histolytica* invasion route in the human colon. Cell Microbiol 14:609–621. https://doi.org/10.1111/j.1462-5822.2012.01752.x.
61. Diamond LS, Harlow DR, Cunnick CC. 1978. A new medium for the axenic cultivation of *Entamoeba histolytica* and other *Entamoeba*. Trans R Soc Trop Med Hyg 72:431–432. https://doi.org/10.1016/0035-9203(78)90144-x.